The University of Alabama in Huntsville

Final Report

Computer Modeling of Inversion Layer MOS Solar Cells and Arrays

(NAG8-083)

Submitted to

George C. Marshall Space Flight Center

National Aeronautics and Space Administration

Marshall Space Flight Center, Alabama 35812

Prepared by

Fat Duen Ho 2/15/91

Fat Duen Ho, Principal Investigator

Associate Professor

Electrical and Computer Engineering

The University of Alabama in Huntsville

Huntsville, Alabama 35899

(205) 895-6168

(NASA-CR-187675) COMPUTER MODELING OF INVERSION LAYER MOS SOLAR CELLS AND ARRAYS Final Technical Progress Report, 31 Dec. 1989 - 30 Jun. 1990 (Alabama Univ.) 75 p CSCL 10A G3/44

N91-17444

Unclas 0330168

ABSTRACT

A two-dimensional numerical model of the inversion-layer metal-insulator-semiconductor (IL/MIS) solar cell is proposed by using finite difference method. The two-dimensional current flow in the device is taken into account in this model. The electrostatic potential distribution, the electron concentration distribution and the hole concentration distribution for different terminal voltages are simulated. The results of sample calculation are presented. The existing problems for this model are addressed. The future work is proposed. In addition, the MIS structures are studied and some of the results are reported.

Introduction

Conventional silicon solar cells using diffused p-n junctions have conversion efficiencies far below the theoretical values of efficiencies (18-22%) [1]. The first major reason is that p-n junction solar cells have high space charge layer recombination which make the I-V characteristics of the cells different from those of ideal junctions. The second major reason is that there are difficulties in controlling very shallow p-n junctions.

Inversion-layer metal-insulator-semiconductor (IL/MIS) solar cells are viable alternatives to conventional diffused p-n junction solar cells. The advantage of IL/MIS cells is that the processing is of low temperature and there is no diffusion-induced crystal damage inherent in diffused p-n junction solar cells. The "dead layer" found at the surface of many p-n junction cells does not exist in IL/MIS devices.

In order to fully understand the operation of an inversion layer solar cell and to have higher efficiency, modeling of IL/MIS cells is needed. So far, however, only several modelings of these devices have been published [2,3,4].

Norman and Thomas [2] have extensively modeled these devices. They introduced a pseudo two-dimensional model. There are two major points in their approach. First, they considered that IL/MIS cells can be treated as a one-dimensional structure. Second, the two dimensional effects are taken into account by electrically connecting these one-dimensional slices in series with the sheet resistance of the inversion layer of the cell. In each one-dimensional slice the semiconductor equations are solved numerically using finite difference method.

Godfrey and Green [3] introduced an important design parameter Δ which characterizes the measured short-circuit current of the IL/MIS solar cell. It can be used to replace the sheet resistance of the inversion layer to determine the spacing of the grid lines for good IL/MIS solar cell performance.

Miller and Olson [4] have developed theoretical models to calculate the IL/MIS cells by solving the two-dimensional steady-state diffusion equation.

However, there exists no two-dimensional model which includes all the two-dimensional semiconductor equations for the IL/MIS solar cells. Our main goal of this study is to develop this model. In our approach we have been trying to solve two-dimensional Poisson's equations, continuity equation for electrons and continuity equation for holes by using finite difference method. The overall objective of the work is to identify and to characterize various mechanisms which tend to limit the conversion efficiency of the IL/MIS solar cells. This will be accomplished through a solution of the fundamental device equations including the effects of the Si-SiO_2 interface charges. An external generation rate due to the full spectrum solar irradiance will also be included.

2. THEORY AND STRUCTURES OF THE IL/MIS SOLAR CELLS

Theory and design consideration for IL/MIS cells have been extensively discussed elsewhere [1]-[4]. The basic structure of an IL/MIS solar cells, shown in Figure 1, consists of a p-Si substrate with a sintered aluminum back contact, a photolithographically defined metal-insulator-semiconductor front contact in the form of a grating, and a thick oxide/antireflection coating. The main function of the oxide in an IL/MIS solar cell is to induce an inversion layer at the surface of the p-Si substrate and to form an ideal n^+-p junction. This inversion layer is formed through the action of positive charges trapped in the oxide during fabrication.

The surface state charge, Q_{ss}, which is considered to be associated with excess silicon close to the SiO_2-Si interface, is the principle charge in thermal oxide, which creates an inversion layer in the regions between the grid lines. Q_{ss} is a direct function of silicon orientation and the oxidation linear rate constant. The value of Q_{ss} is highest on <111> oriented substrates and can be changed over a wide range by heat treatment in dry oxygen. Q_{ss} also depends on the oxidizing ambient final temperature. The values of Q_{ss} increase with decreasing temperature. The process of oxide annealing for a particular time in an ambient with different chemicals will also affect the values of Q_{ss} [5].

The minority carriers (electrons in this case) generated in the p-type silicon substrate are collected vertically and then flow along the inversion layer to the MIS contacts, which is shown in Figure 2. In order to collect electrons more effectively we have to place the MIS contacts close enough to ensure that minority carriers can be collected by the contacts. Typically, the MIS contacts are spaced in a distance which is close to the values of diffusion length of the minority carriers (50-120 micrometers). To optimize the trade-off between grid shading and high sheet resistance in the inversion layer of the cell, we should carefully choose the grid finger spacing.

One of the most important parts of the inversion layer MIS cell is the MIS contact. Thin oxide layers can be grown in the contact windows. Unlike thin metal MIS solar cells, the grid MIS contact used in IL/MIS cells is always under dark conditions due to the thickness of the metal on the top of the thin oxide layer. Since MIS contacts are very important a detailed study is needed to characterize these grid diodes. The MIS structures under solar irradiance conditions have been investigated. The research results are in Appendix A. For calculation of dark currents the analytical model used in Appendix A is still valid if the terms of the expressions in this model, which are related to sunlight, are removed. The detailed calculations and the numerical results for the study of the MIS contacts under dark conditions will be presented in subsequent reports of a full account of this work.

3. NUMERICAL MODEL

3.1 Semiconductor Equations

Poisson's equation can be written as

$$\nabla^2\psi = -\frac{q}{\epsilon}(p - n + N_d - N_a) \tag{1}$$

where ψ is the electrostatic potential, p and n are hole and electron concentrations, and N_d and N_a are the ionized donor and acceptor concentrations. The steady-state continuity equations for electrons and holes, respectively, are given by

$$\frac{1}{q}\vec{\nabla} \cdot \vec{J}_n = -G_n + R_n \tag{2}$$

$$\frac{1}{q}\vec{\nabla} \cdot \vec{J}_p = G_p - R_p \tag{3}$$

The electron and hole transport equations can be expressed by

$$\vec{J}_n = -q\,\mu_n n\,\vec{\nabla}\psi + q\,D_n\,\vec{\nabla}n \tag{4}$$

$$\vec{J}_p = -q\,\mu_p p\,\vec{\nabla}\psi - q\,D_p\,\vec{\nabla}p \tag{5}$$

In eqs. (2) and (3) R_n and R_p are the net recombination rates of electrons and holes, respectively. G_n and G_p are photogeneration rate of electrons and holes, respectively.

If we assume that $G_n = G_p = G$, then the generation rate in the IL/MIS cell is calculated by

$$G(x) = \int_0^{\infty} [1 - R(\lambda)]\,\alpha(\lambda) N_m(\lambda) \exp[-\alpha(\lambda)x]d\lambda \tag{6}$$

where $N_m(\lambda)$ represents the incident photon density or the air mass m photon flux spectrum, $R(\lambda)$ is the optical reflection of the IL/MIS cell's front surface at wavelength λ, $\alpha(\lambda)$ is the absorption coefficient, and the integration includes all wavelengths in the solar spectrum (from λ = 200 nm to λ = 1200 nm) with energy greater than the bandgap of silicon.

The recombination rate is described by the Shocky-Read-Hall recombination theory via trapping center, which can be written as

$$R = \frac{pn - n_i^2}{(n+n_i)\,\tau_p + (p+n_i)\tau_n} \tag{7}$$

where τ_p and τ_n are the hole and electrons lifetimes which depend on the positions. In the bulk eq. (7) can be simplified to

$$R = \frac{n}{\tau_n} \tag{8}$$

where τ_n can be assumed to be a constant.

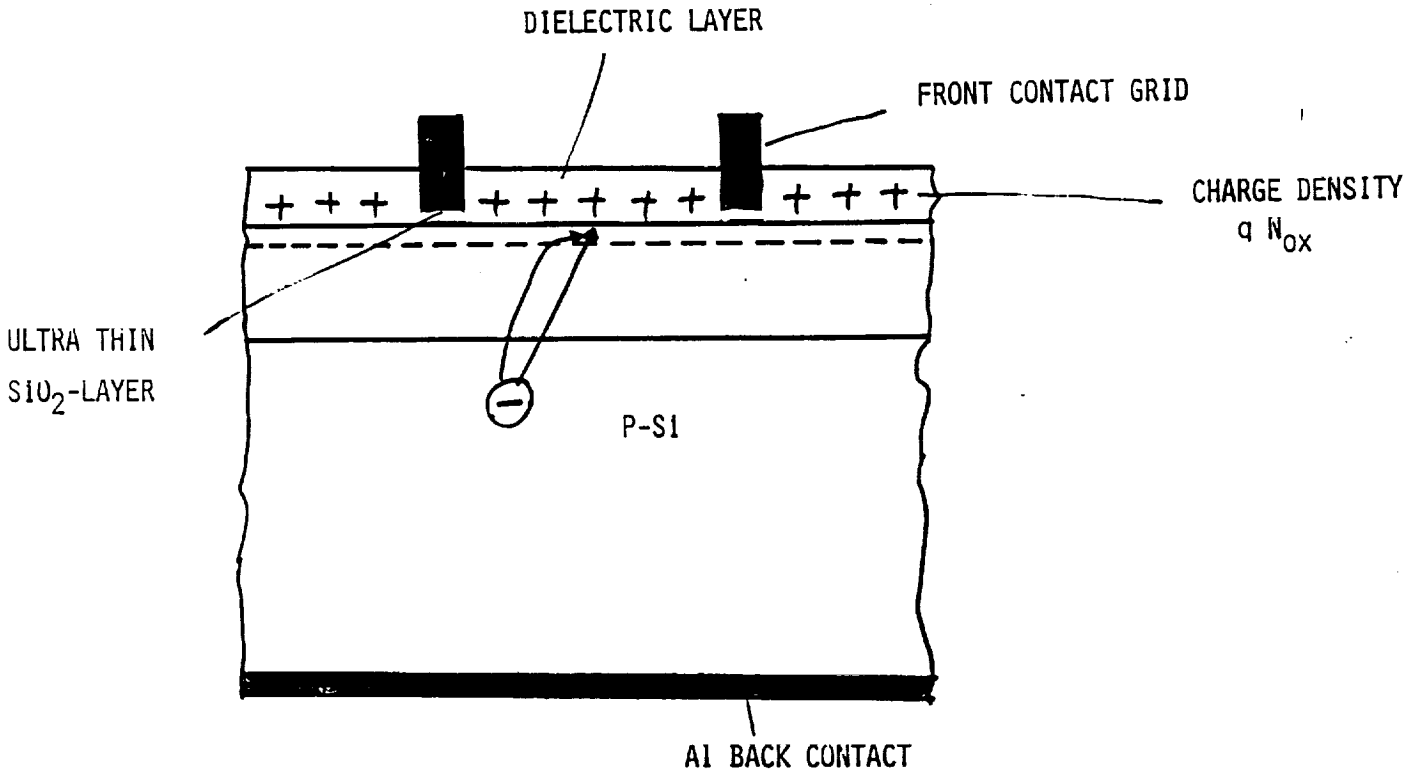

Figure 1. Schematic Cross Section of an IL/MIS Solar Cell

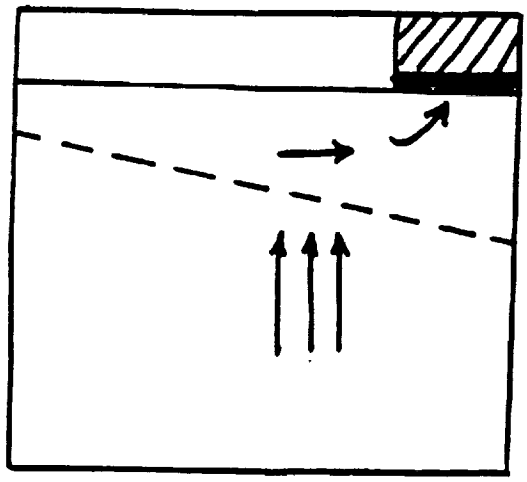

Figure 2. Schematic Diagram of the Electron Current Flow in an MIS Inversion Layer Solar Cell

3.2 Discretization of the Semiconductor Equations with Finite Differences

Since the numerical values of the variables (ψ,n,p,etc.) in the semiconductor equations are quite different in orders of magnitude, we need to normalize them by a set of scaling factors introduced by DeMari [6,7], which is shown in Table 1.

TABLE 1. Scaling Factors

Quantity	Scaling Factor
Position or length	$L_D \triangleq (\epsilon_s kT/q^2 n_i)^{\frac{1}{2}}$ (cm)
Potential	$V_T \triangleq kT/q$ (V)
Carrier/impurity concentration	n_i (cm^{-3})
Diffusion Coefficient	1 cm^2 S^{-1}

The node structure used in this work is rectangular with nonuniform spacing in the horizontal and vertical directions, which is shown in Figure 3. The continuous form of Poisson's equation in two dimensions can be approximated by the difference equation which can be expressed by

$$\frac{h_i + h_{i-1}}{2k_{j-1}} \psi_{i,j-1} + \frac{k_j + k_{j-1}}{2h_{i-1}} \psi_{i-1,j}$$

$$- \left[\frac{k_j + k_{j-1}}{2h_i} + \frac{k_j + k_{j-1}}{2h_{i-1}} + \frac{h_i + h_{i-1}}{2k_j} + \frac{h_i + h_{i-1}}{2k_{j-1}} \right] \psi_{i,j}$$

$$+ \frac{k_j + k_{j-1}}{2h_i} \psi_{i+1,j} + \frac{h_i + h_{i-1}}{2k_j} \psi_{i,j+1}$$

$$- (n_{i,j} - p_{i,j} - N_{i,j}) \frac{h_i + h_{i-1}}{2} \cdot \frac{k_j + k_{j-1}}{2} = 0 \qquad (9)$$

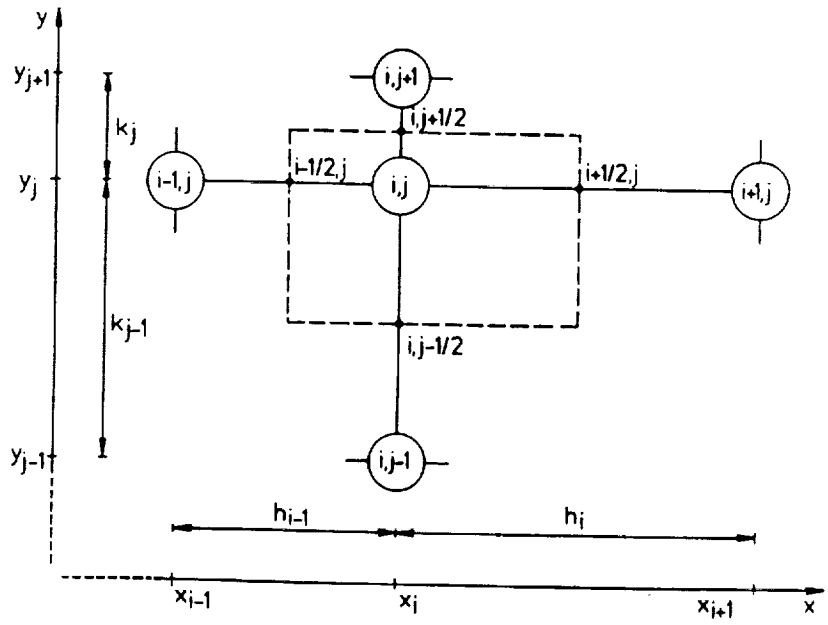

Figure 3. A Node and its Four Adjacent Neighbors Used in the Expressions of the Finite Difference Formulation.

The discretized form of continuity equation for electrons can be written as

$$
\begin{aligned}
&- n_{i,j-1} D_n \Big|_{i,j-\frac{1}{2}} B(\psi_{i,j-1} - \psi_{i,j}) \frac{h_{i-1} + h_i}{2k_{j-1}} \\
&- n_{i,j} D_n \Big|_{i-\frac{1}{2},j} B(\psi_{i-1,j} - \psi_{i,j}) \frac{k_{j-1} + k_j}{2h_{i-1}} \\
&+ n_{i,j} \Big[D_n \Big|_{i,j-\frac{1}{2}} B(\psi_{i,j} - \psi_{i,j-1}) \frac{h_{i-1} + h_i}{2k_{j-1}} \\
&\quad + D_n \Big|_{i-\frac{1}{2},j} B(\psi_{i,j} - \psi_{i-1,j}) \frac{k_{j-1} + k_j}{2h_{i-1}} \\
&\quad + D_n \Big|_{i+\frac{1}{2},j} B(\psi_{i,j} - \psi_{i-1,j}) \frac{k_{j-1} + k_j}{2h_i} \\
&\quad + D_n \Big|_{i,j+\frac{1}{2}} B(\psi_{i,j} - \psi_{i,j+1}) \frac{h_{i-1} + h_i}{2k_j} \Big] \\
&- n_{i+1,j} D_n \Big|_{i+\frac{1}{2},j} B(\psi_{i+1,j} - \psi_{i,j}) \frac{k_{j-1} + k_j}{2h_i} \\
&- n_{i,j+1} D_n \Big|_{i,j+\frac{1}{2}} B(\psi_{i,j+1} - \psi_{i,j}) \frac{h_{i-1} + h_i}{2k_j} \\
&+ R_{i,j} \frac{(h_{i-1} + h_i)(k_{j-1} + k_j)}{4} - G_{i,j} \frac{(h_{i-1} + h_i)(k_{j-1} + k_j)}{4} = 0
\end{aligned}
\tag{10}
$$

where B(x) is the Bernouli function which is given by

$$
B(x) = \frac{x}{e^x - 1} \tag{11}
$$

Similarly, we can write the discretized continuity equation for holes

3.3 Discretization of Boundary Equations

At the interface between the semiconductor and oxide we can apply Gauss' law in differential form to the boundary and obtain

$$
\epsilon_{si} \frac{\partial \psi}{\partial \vec{n}} \Big|_{si} - \epsilon_{ox} \frac{\partial \psi}{\partial \vec{n}} \Big|_{ox} - Q_{ss} = 0 \tag{12}
$$

$\vec{n}$ denotes the unit normal vector on the interface, and ϵ_{si} and ϵ_{ox} are the permittivity of silicon and oxide, respectively. Q_{ss} represents the interface charges. Using y to replace $\vec{n}$ we have

$$G_{si} \frac{\partial \psi}{\partial y}\Big|_{si} - \epsilon_{ox} \frac{\partial \psi}{\partial y}\Big|_{ox} - Q_{ss} = 0 \tag{13}$$

Scaling the above equation we have

$$\epsilon_{si} \frac{\partial \psi}{\partial y}\Big|_{si} - \epsilon_{ox} \frac{\partial \psi}{\partial y}\Big|_{ox} - Q_{INT} = 0 \tag{14}$$

and

$$Q_{INT} = Q_{ss} \frac{x_o}{y_o} \tag{15}$$

where $x_o = \sqrt{\epsilon_s kT/q^2 n_i}$ and $\psi_o = \frac{kT}{q}$, which are scaling factors.

The partial derivatives can be expressed by difference expressions and can be written as

$$\frac{\partial \psi}{\partial y}\Big|_{si}\Big|_{i,j} = \frac{\psi_{i,j} - \psi_{i,j-1}}{k_{j-1}} + \frac{k_{j-1}}{2} \frac{\partial^2 \psi}{\partial y^2}\Big|_{si}\Big|_{i,j} \tag{16}$$

$$\frac{\partial \psi}{\partial y}\Big|_{ox}\Big|_{i,j} = \frac{\psi_{i,j+1} - \psi_{i,j}}{k_j} - \frac{k_j}{2} \frac{\partial^2 \psi}{\partial y^2}\Big|_{ox}\Big|_{i,j} \tag{17}$$

where

$$\frac{\partial^2 \psi}{\partial y^2}\Big|_{si}\Big|_{i,j} = -\left[\frac{\frac{\psi_{i+1,j} - \psi_{i,j}}{h_i} - \frac{\psi_{i,j} - \psi_{i-1,j}}{h_{i-1}}}{\frac{h_{i-1} + h_i}{2}} \right] + n_{i,j} - p_{i,j} - N_{i,j} \tag{18}$$

$$\frac{\partial^2 \psi}{\partial y^2}\Big|_{ox}\Big|_{i,j} = -\left[\frac{\frac{\psi_{i+1,j} - \psi_{i,j}}{h_i} - \frac{\psi_{i,j} - \psi_{i-1,j}}{h_{i-1}}}{\frac{h_{i-1} + h_i}{2}} \right] \tag{19}$$

Substituting Eqs. (18) and (19) into Eqs. (16) and (17), respectively, and rearranging Eq. (14), we obtain

$$\epsilon_{si}\left[\frac{\psi_{i,j}-\psi_{i,j-1}}{k_{j-1}}+\frac{k_{j-1}}{2}\left\{-\frac{\frac{\psi_{i+1,j}-\psi_{i,j}}{h_i}-\frac{\psi_{i,j}-\psi_{i-1,j}}{h_{i-1}}}{\frac{h_{i-1}+h_i}{2}}\right]+n_{i,j}-p_{i,j}-N_{i,j}\right\}\right]$$

$$-\epsilon_{ox}\left[\frac{\psi_{i,j+1}-\psi_{i,j}}{k_j}-\frac{k_j}{2}\left\{-\frac{\frac{\psi_{i+1,j}-\psi_{i,j}}{h_i}-\frac{\psi_{i,j}-\psi_{i-1,j}}{h_{i-1}}}{\frac{h_{i-1}+h_i}{2}}\right\}\right]-Q_{INT}\Big|_{i,j}=0 \quad (20)$$

Rearranging Eq. (20) leads to

$$\psi_{i,j-1}\frac{h_{i-1}+h_i}{2k_{j-1}}\epsilon_{si}+\psi_{i-1,j}\frac{\epsilon_{si}k_{j-1}+\epsilon_{ox}k_j}{2k_{j-1}}$$

$$-\psi_{i,j}\left[\frac{h_{i-1}+h_i}{2k_{j-1}}\epsilon_{si}+\frac{\epsilon_{si}k_{j-1}+\epsilon_{ox}k_j}{2h_{i-1}}+\frac{\epsilon_{si}k_{j-1}+\epsilon_{ox}k_j}{2h_i}+\frac{h_{i-1}+h_i}{2k_j}\epsilon_{ox}\right]$$

$$+\psi_{i+1,j}\frac{\epsilon_{si}k_{j-1}+\epsilon_{ox}k_j}{2h_i}+\psi_{i,j+1}\frac{h_{i-1}+h_i}{2k_j}\epsilon_{ox}$$

$$-(n_{i,j}-p_{i,j}-N_{i,j})\left[\frac{h_{i-1}+h_i}{2}\right]\left[\frac{\epsilon_{si}k_{j-1}}{2}\right]$$

$$+\frac{h_{i-1}+h_i}{2}Q_{INT}\Big|_{i,j}=0 \quad (21)$$

At the oxide–semiconductor interface, the discrete form of the steady–state continuity equation for electrons can be written as

$$-n_{i,j-1}D_n\Big|_{i,j-\frac{1}{2}}B(\psi_{i,j-1}-\psi_{i,j})\frac{h_{i-1}+h_i}{2k_{j-1}}$$

$$-n_{i-1,j}D_n\Big|_{i-\frac{1}{2},j}B(\psi_{i-1,j}-\psi_{i,j})\frac{k_{j-1}}{2h_{i-1}}$$

$$+n_{i,j}\left[D_n\Big|_{i,j-\frac{1}{2}}B(\psi_{i,j}-\psi_{i,j-1})\frac{h_{i-1}+h_i}{2k_{j-1}}\right.$$

$$+ D_n\Big|_{i-\frac{1}{2},j} B(\psi_{i,j} - \psi_{i-1,j}) \frac{k_{j-1}}{2h_{i-1}}$$

$$+ D_n\Big|_{i+\frac{1}{2},j} B(\psi_{i,j} - \psi_{i+1,j}) \frac{k_{j-1}}{2h_i} \Big]$$

$$- n_{i+1,j} D_n\Big|_{i+\frac{1}{2},j} B(\psi_{i+1,j} - \psi_{i,j}) \frac{k_{j-1}}{2h_i}$$

$$= - R_{i,j} \frac{h_{i-1} + h_i}{2} \cdot \frac{k_{j-1}}{2} + G_{i,j} \frac{h_{i-1} + h_i}{2} \cdot \frac{k_{j-1}}{2} \tag{22}$$

Similarly we can obtain the discrete form of continuity equation for holes at the interface.

The discretized Poisson's equation at the left–size wall of the device can be derived as follows:

$$\frac{\partial \psi}{\partial x}\Big|_{i-\frac{1}{2},j} = 0 = \frac{\frac{\partial \psi}{\partial x}\Big|_{i+\frac{1}{2},j} + \frac{\partial \psi}{\partial x}\Big|_{i-\frac{1}{2},j}}{2} \tag{23}$$

From the above equation we obtain

$$\frac{\partial \psi}{\partial x}\Big|_{i-\frac{1}{2},j} = - \frac{\partial \psi}{\partial x}\Big|_{i+\frac{1}{2},j} \tag{24}$$

Let $h_0 = h_i$, then $\frac{h_i + h_{i-1}}{2} = h_i$. Poisson's equation at the left–side wall becomes

$$- \frac{h_i}{2k_{j-1}} \psi_{i,j-1} + \left[\frac{k_{j-1}+k_j}{2h_i} + \frac{h_i}{2k_j} + \frac{h_i}{2k_{j-1}} \right] \psi_{i,j} - \frac{k_{j-1}+k_j}{2h_i} \psi_{i+1,j} - \frac{h_i}{2k_j} \psi_{i,j+1}$$

$$+ (n_{i,j} - p_{i,j} - N_{i,j}) \left[\frac{h_i}{2} \right] \left[\frac{k_{j-1}+k_j}{2} \right] = 0 \tag{25}$$

Similarly, at the right–size wall of the device, the discretized Poisson's equation becomes

$$- \frac{h_{i-1}}{2k_{j-1}} \psi_{i,j-1} - \frac{k_{j-1}+k_j}{2h_{i-1}} \psi_{i-1,j} + \left[\frac{k_{j-1}+k_j}{2h_{i-1}} + \frac{h_{i-1}}{2k_j} + \frac{h_{i-1}}{2k_{j-1}} \right] \psi_{i,j}$$

$$- \frac{h_{i-1}}{2k_j} \psi_{i,j+1} + + (n_{i,j} - p_{i,j} - N_{i,j}) \left[\frac{h_{i-1}}{2} \right] \left[\frac{k_{j-1}+k_j}{2} \right] = 0 \tag{26}$$

At the left–side and the right–side walls the following boundary condition holds:

$$\vec{J}_n \cdot \vec{n} = 0 \tag{27}$$

$$\vec{J}_p \cdot \vec{n} = 0 \tag{28}$$

or

$$J_{nx}\Big|_{i,j} = 0 \tag{29}$$

$$J_{px}\Big|_{i,j} = 0 \tag{30}$$

Eq. (29) can be interpreted as

$$\frac{J_{nx}\Big|_{i+\frac{1}{2},j} + J_{nx}\Big|_{i-\frac{1}{2},j}}{2} = 0 \tag{31}$$

or

$$J_{nx}\Big|_{i+\frac{1}{2},j} = -J_{nx}\Big|_{i-\frac{1}{2},j} = 0 \tag{32}$$

Finally, at the left–side wall the discretized continuity equation for electrons can be written as

$$\begin{aligned}
&- n_{i,j-1} D_n\Big|_{i,j-\frac{1}{2}} B(\psi_{i,j-1} - \psi_{i,j}) \frac{h_i}{2k_{j-1}} \\
&+ n_{i,j}\Big[D_n\Big|_{i,j-\frac{1}{2}} B(\psi_{i,j} - \psi_{i,j-1}) \frac{h_i}{2k_{j-1}} \\
&\quad + D_n\Big|_{i+\frac{1}{2},j} B(\psi_{i,j} - \psi_{i+1,j}) \frac{k_{j-1}+k_j}{2h_i} \\
&\quad + D_n\Big|_{i,j+\frac{1}{2}} B(\psi_{i,j} - \psi_{i,j+1}) \frac{h_i}{2k_j} \Big] \\
&- n_{i+1,j} D_n\Big|_{i+\frac{1}{2},j} B(\psi_{i+1,j} - \psi_{i,j}) \frac{k_{j-1}+k_j}{2h_i} \\
&- n_{i,j+1} D_n\Big|_{i,j+\frac{1}{2}} B(\psi_{i,j+1} - \psi_{i,j}) \frac{h_i}{2k_j} \\
&+ R_{i,j} \left[\frac{h_i}{2}\right] \left[\frac{k_{j-1}+k_j}{2}\right] - G_{i,j} \left[\frac{h_i}{2}\right] \left[\frac{k_{j-1}+k_j}{2}\right] = 0
\end{aligned} \tag{33}$$

Similarly, we can obtain the discrete form of continuity equation for holes at the left–side wall. The same discretization procedure can be applied to the right–side wall of the device.

3.4 Gummel's Method

Gummel's method [8] is the most commonly used method for getting consistent solutions to the semiconductor equations (the Poisson's equation and continuity equations). This method can be described as follows:

1. Beginning with an initial approximation $\psi^{(0)}$ in the electrostatic potential and initial values of carrier concentrations ($n^{(-1)}$ and $p^{(-1)}$), the Poisson's equation is solved for ψ.
2. Using the new potential and appropriate carrier statistics (Boltzmann or Fermi–Dirac) the values of n and p are updated and the Poisson's equation is solved again. These computations are repeated until the potential change is below the tolerance.
3. In the previous step we assume that the quasi–Fermi level is fixed for updating the values of n and p. In fact we must calculate the quasi– Fermi level because it is unknown. This is done by the continuity equations and updating the values of n and p without changing the potentials.
4. Using the new values of n and p the Poisson's equation is solved again.
5. Finally potentials and the values of n and p converge and are consistent with the Poisson's equation and with the continuity equations.

In summary, this decoupled approach requires

a) the solution of Poisson's equation

b) the solution of linearized Poisson's equation

c) the solution of continuity equation for electrons

d) the solution of continuity equation for holes.

3.5 Solutions of the Linearized Discrete Equations

To solve the large set of algebraic equations in two or three dimensional approximation we need to select more effective iterative method. In this calculation Stone's strongly implicit method [9] is used. The important points of this method are

a. Modification of the matrix form from five non–zero diagonals to seven non–zero diagonals.

b. Generation of new set of intermediate coefficients for fast convergence.

c. Use of varying acceleration parameters depending on the number of grids.

d. Double sweep procedures with same parameters from left down corner and from right up corner of the model.

4. RESULTS AND DISCUSSIONS

We have used 12 (horizontal) × 50 (vertical) meshes to model the IL/MIS solar cell. Its depth is 200 μm and its width is 300 μm. Horizontally, we only modeled up to the middle of the cell due to the symmetry of the grid structure.

Figures 4, 7, and 10 show the electrostatic potential distributions in the solar cell for terminal voltages 0.3V, 0.4V and 0.5V, respectively. Figures 5, 8, and 11 demonstrate the concentrations of electrons for 0.3V, 0.4V and 0.5V, respectively. The hole concentrations for the terminal voltages 0.3V, 0.4V and 0.5V are shown in Figure 5, 8, and 11, respectively. The respective data for these figures are in Appendix B.

Figures 5, 8, and 11 demonstrate that the inversion layers are clearly formed at the Si–SiO_2 interface. The electrostatic potential distributions are reasonable for lower terminal voltages (0.3V and below). However, for the terminal voltages 0.4V and 0.5V the surface electrostatic potentials from the left–side wall to the right increase first then decrease as they approach to the middle of the IL/MIS cell. Efforts have been made to solve this problem before calculating the currents.

In summary we have set up a two–dimensional numerical model for IL/MIS solar cells. This is a time consuming and difficult task. The values of electron concentrations and the hole concentrations obtained from our numerical model are reasonable. Good results are also obtained for electrostatic potentials for lower terminal voltages. The future work should be centered on the above-mentioned problems and calculate the currents to obtain I–V characteristics for the IL/MIS solar cell. Using our numerical model the design of the cell should be optimized by changing the values of the parameters, such as the Si–SiO_2 interface changes, the dopant concentrations of the wafers, the grid line densities, the thickness of the wafers, etc. In addition, we should study MIS structures more, especially in dark conditions.

ELECTROSTATIC POTENTIAL DISTRIBUTION

TERMINAL VOLTAGE= 0.30 V

AMPLITUDES ARE IN VOLTS

VERTICAL/HORIZONTAL POINTS REPRESENT MESHES

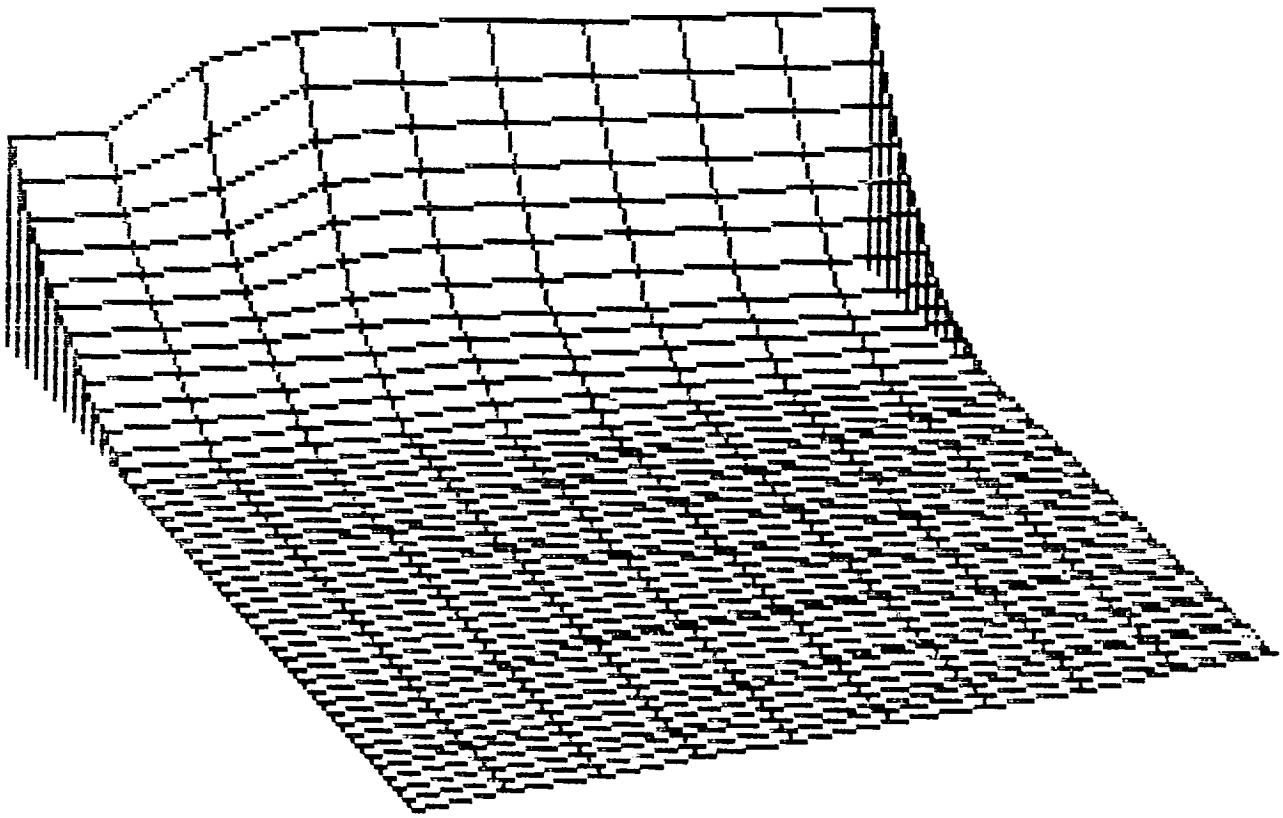

Figure 4. Electrostatic Potential Distribution for the IL/MIS Solar Cell at Terminal Voltage Equal to 0.3V.

ELECTRON CONCENTRATION DISTRIBUTION

TERMINAL VOLTAGE- 0.30 V
AMPLITUDES ARE IN LOGARITHM SCALE
VERTICAL/HORIZONTAL POINTS REPRESENT MESHES

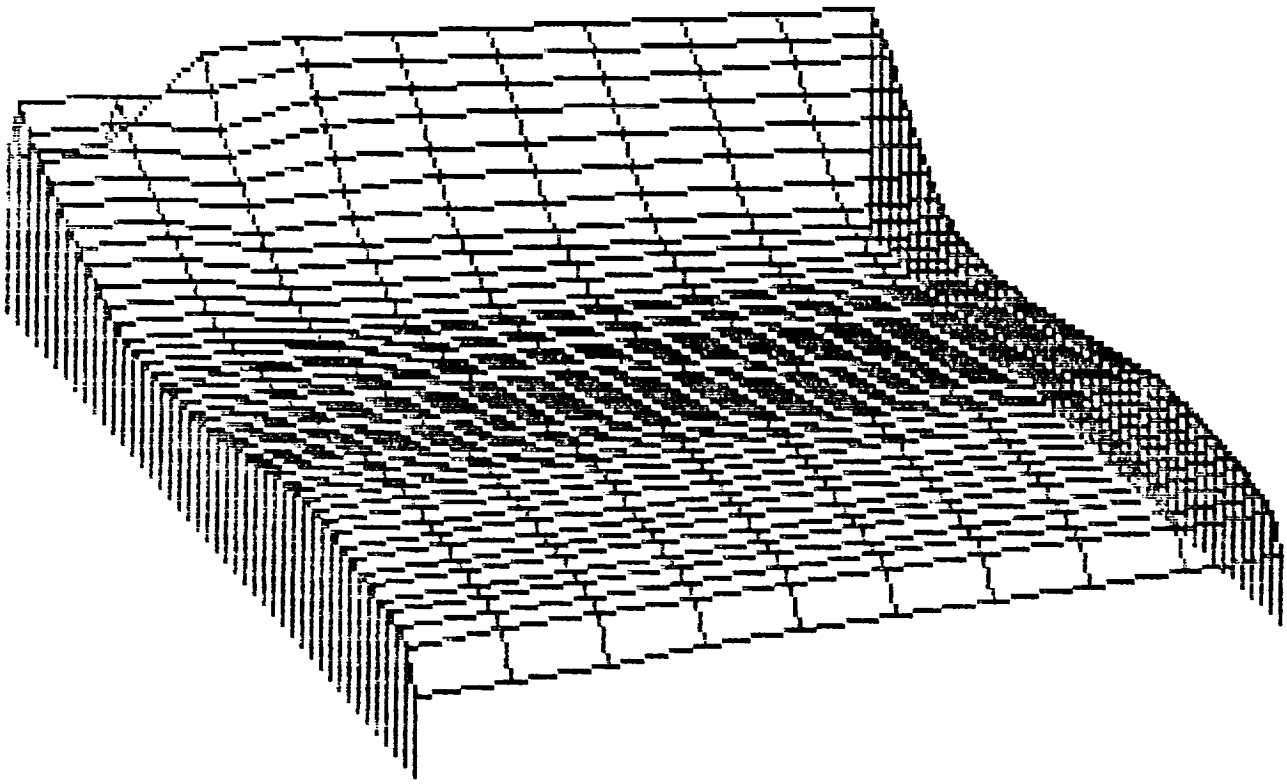

Figure 5. Electron Concentration Distribution for the IL/MIS Solar Cell at Terminal Voltage Equal to 0.3V.

HOLE CONCENTRATION DISTRIBUTION

TERMINAL VOLTAGE= 0.30 V
AMPLITUDES ARE IN LOGARITHM SCALE
VERTICAL/HORIZONTAL POINTS REPRESENT MESHES

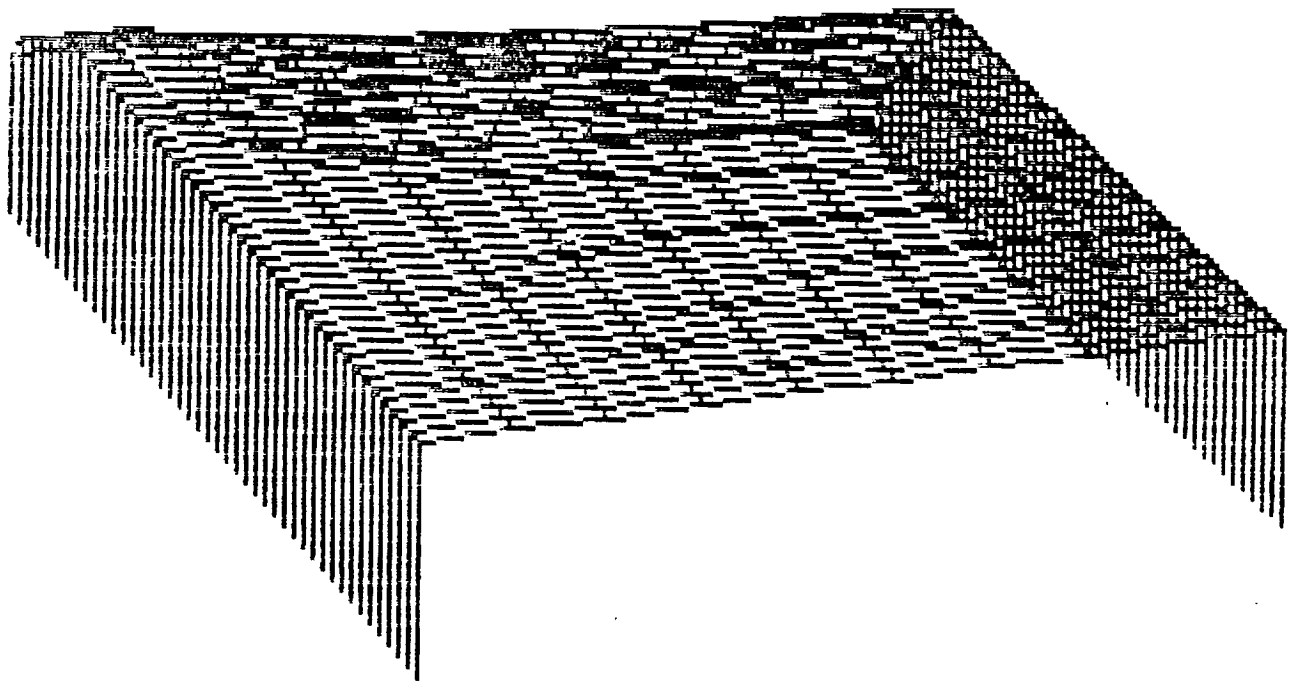

Figure 6. Hole Concentration Distribution for the IL/MIS Solar Cell at Terminal Voltage Equal to 0.3V.

ELECTROSTATIC POTENTIAL DISTRIBUTION

TERMINAL VOLTAGE= 0.40 V

AMPLITUDES ARE IN VOLTS

VERTICAL/HORIZONTAL POINTS REPRESENT MESHES

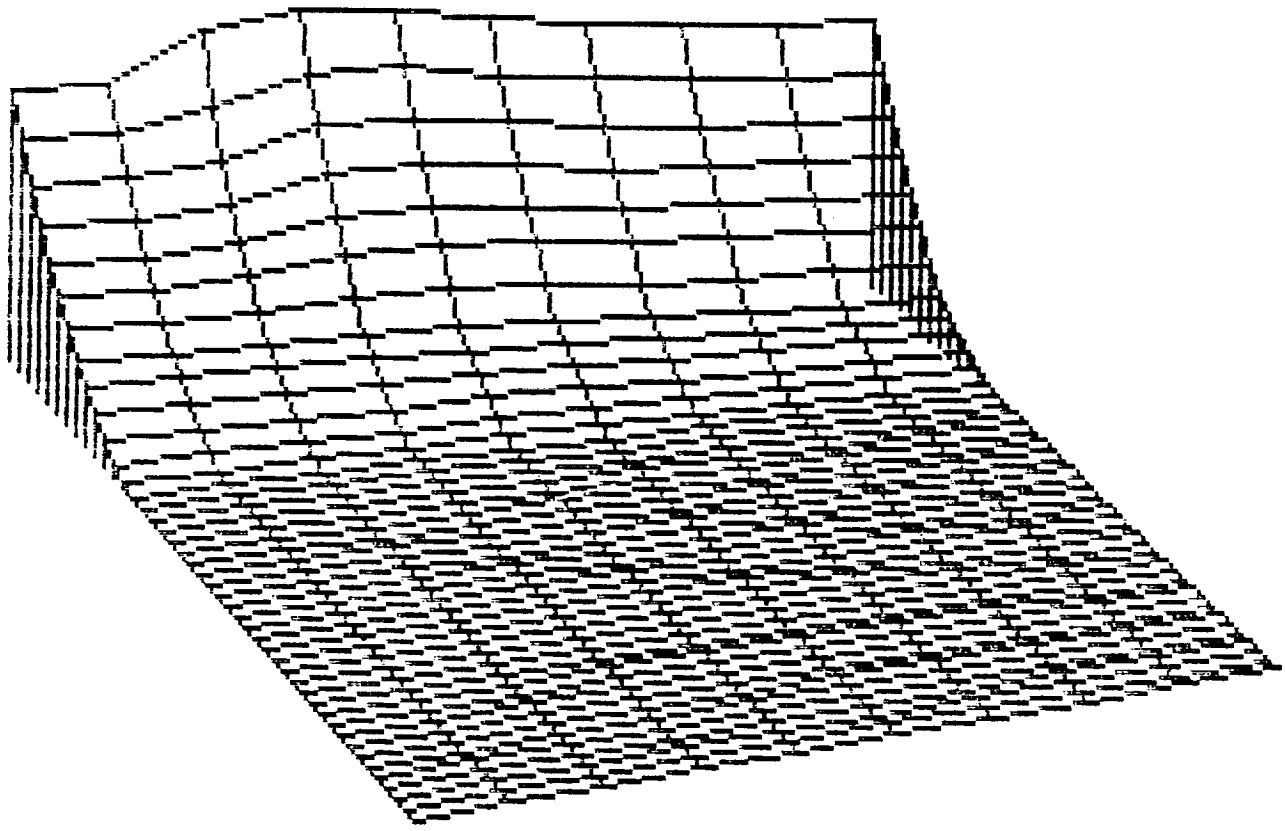

Figure 7. Electrostatic Potential Distribution for the IL/MIS Solar Cell at Terminal Voltage Equal to 0.4V.

ELECTRON CONCENTRATION DISTRIBUTION

TERMINAL VOLTAGE= 0.40 V
AMPLITUDES ARE IN LOGARITHM SCALE
VERTICAL/HORIZONTAL POINTS REPRESENT MESHES

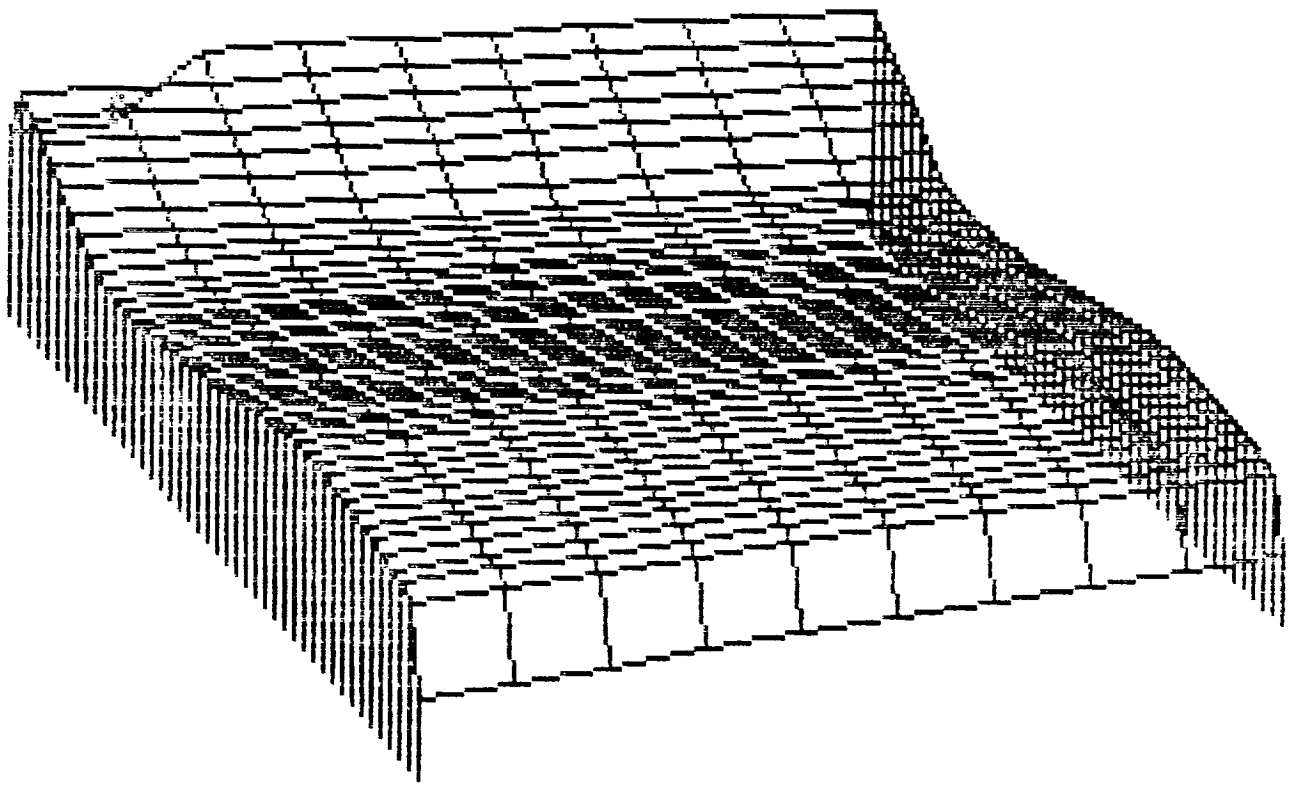

Figure 8. Electron Concentration Distribution for the IL/MIS Solar Cell at Terminal Voltage Equal to 0.4V.

HOLE CONCENTRATION DISTRIBUTION

TERMINAL VOLTAGE= 0.40 V
AMPLITUDES ARE IN LOGARITHM SCALE
VERTICAL/HORIZONTAL POINTS REPRESENT MESHES

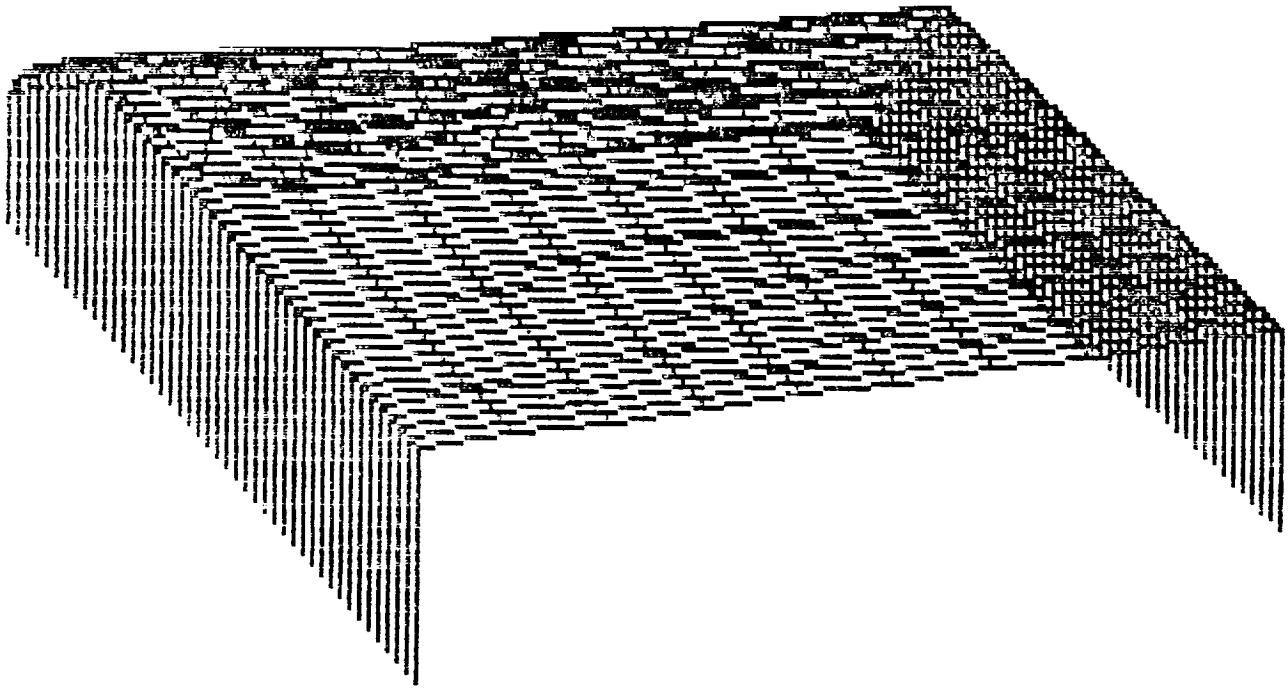

Figure 9. Hole Concentration Distribution for the IL/MIS Solar Cell at Terminal Voltage Equal to 0.4V.

ELECTROSTATIC POTENTIAL DISTRIBUTION

TERMINAL VOLTAGE= 0.50 V

AMPLITUDES ARE IN VOLTS

VERTICAL/HORIZONTAL POINTS REPRESENT MESHES

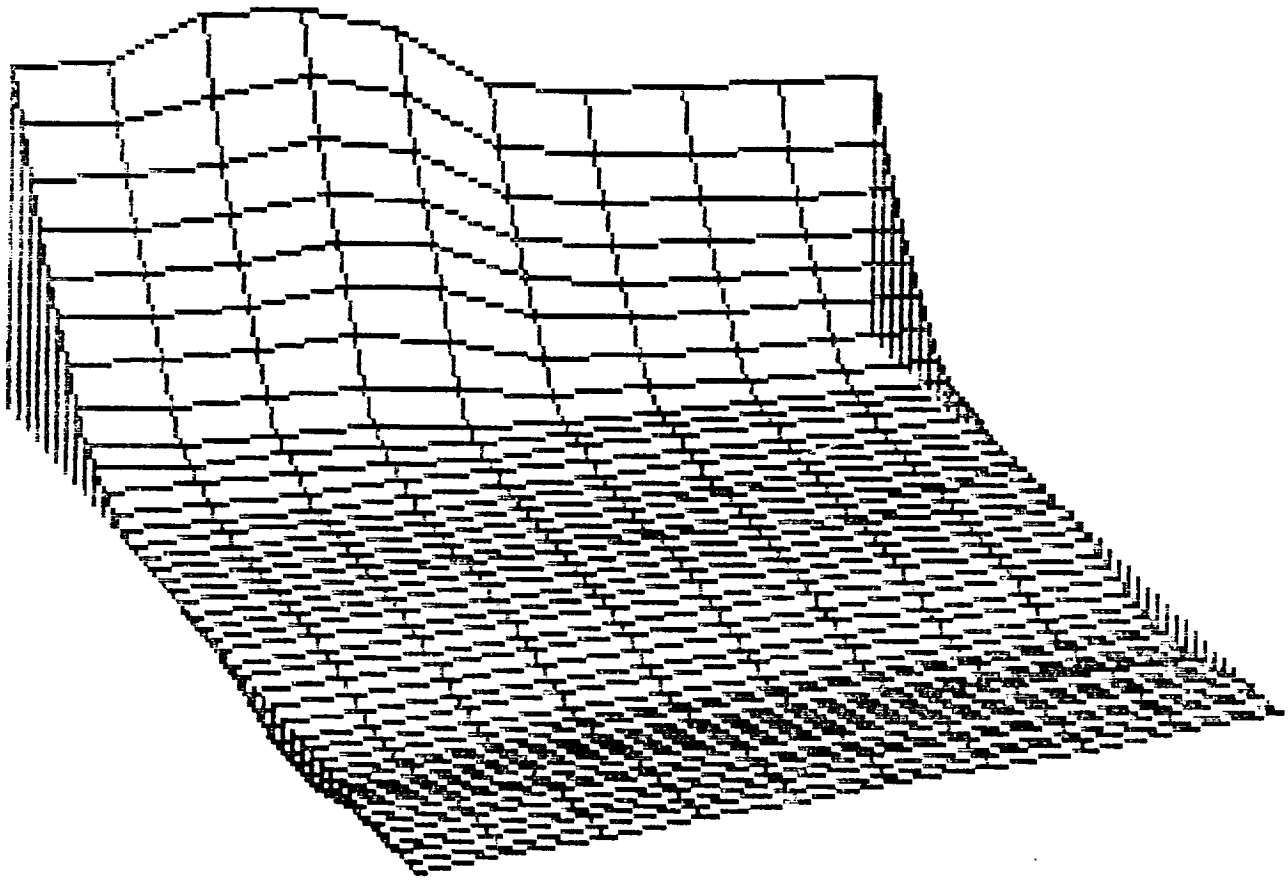

Figure 10. Electrostatic Potential Distribution for the IL/MIS Solar Cell at Terminal Voltage Equal to 0.5V.

ELECTRON CONCENTRATION DISTRIBUTION

TERMINAL VOLTAGE- 0.50 V
AMPLITUDES ARE IN LOGARITHM SCALE
VERTICAL/HORIZONTAL POINTS REPRESENT MESHES

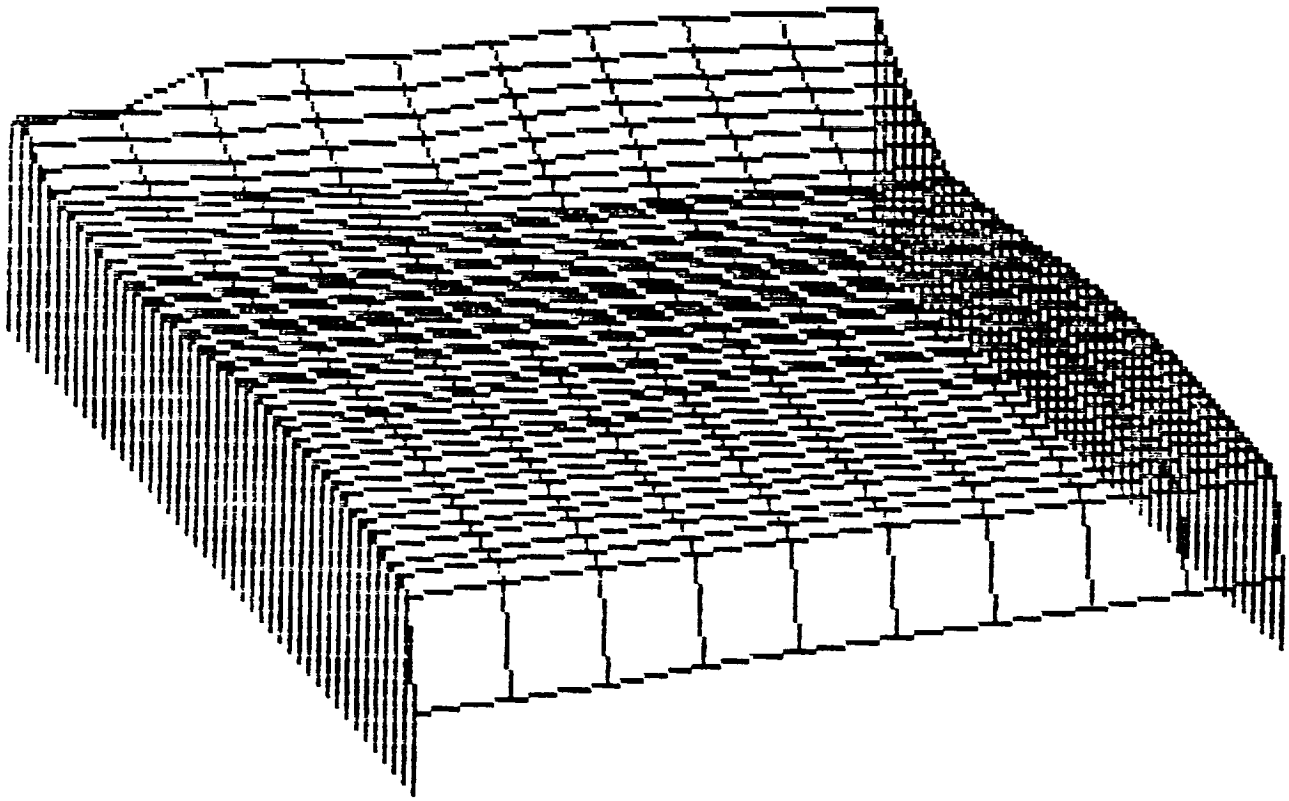

Figure 11. Electron Concentration Distribution for the IL/MIS Solar Cell at Terminal Voltage Equal to 0.5V.

HOLE CONCENTRATION DISTRIBUTION

TERMINAL VOLTAGE= 0.50 V
AMPLITUDES ARE IN LOGARITHM SCALE
VERTICAL/HORIZONTAL POINTS REPRESENT MESHES

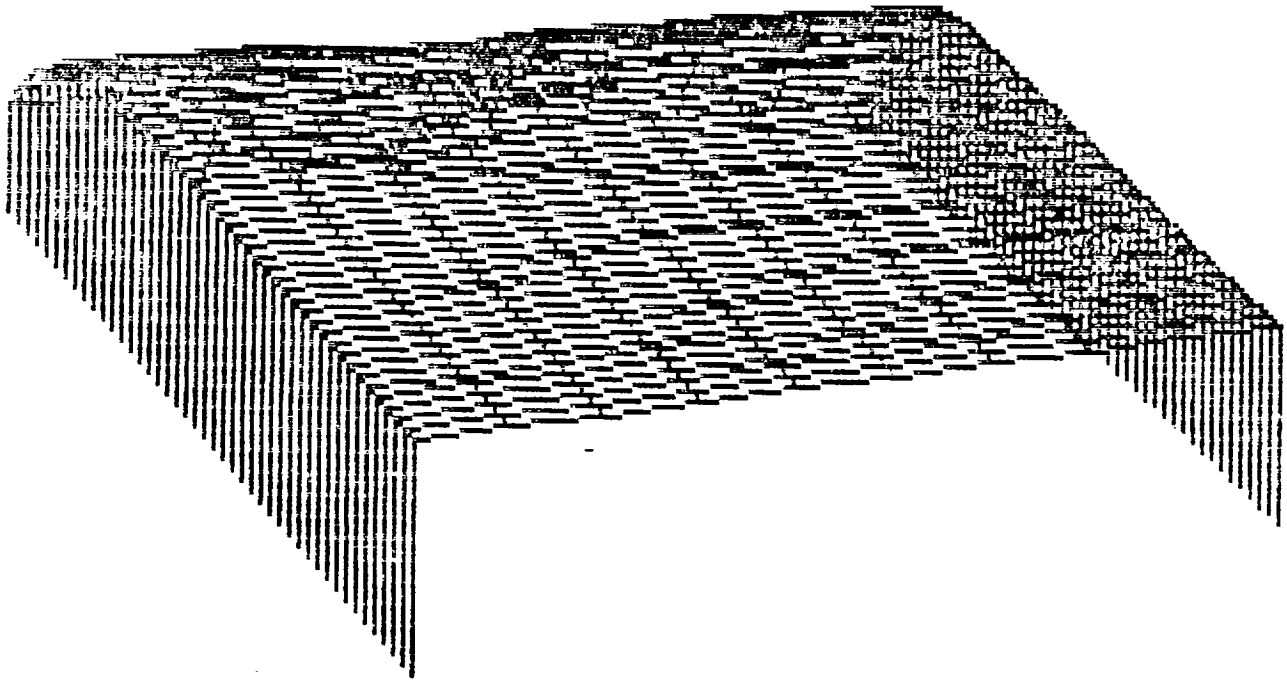

Figure 12. Hole Concentration Distribution for the IL/MIS Solar Cell at Terminal Voltage Equal to 0.5V.

APPENDIX A

A Comprehensive Analytical Model for Metal–Insulator–Semiconductor (MIS) Solar Cells

A Comprehensive Analytical Model for Metal-Insulator-Semiconductor (MIS) Solar Cells

by

M. Y. Doghish and Fat Duen Ho
Department of Electrical and Computer Engineering
The University of Alabama in Huntsville
Huntsville, Alabama 35899

Abstract

A comprehensive model for MIS (Metal-Insulator-Semiconductor) solar cells has been developed which consists of a wide range of parameters. The parameters neglected by other authors have been included. The effects of surface states, silicon dioxide thickness, substrate doping, fixed oxide charges, substrate thickness, and metal work function are all taken into account. This model uses the actual spectrum of sun light (AM1) and assumes a double layer antireflection coating (DLAR) to calculate the open circuit voltages, the short-circuit currents, the fill factors, and the efficiencies of the MIS solar cells.

Nomenclature

$A_n^*(A_p^*)$ = effective Richardson constant for electrons (holes)

d_i = oxide thickness

D_n = diffusion coefficient for electrons

D_{it} = density of surface states (states/cm^2-eV)

$F_t(F_{to})$ = surface states occupation probability with (without) tunneling current through the surface states.

f_m = occupation probability of an energy level equal to E_{ss} in the metal.

F_o = number of incident photons/cm^2.s per unit band width

H = thickness of the cell

n_{p_o} = electron concentration in neutral region of semiconductor, $n_{p_o} = \frac{n_i^2}{N_A}$

L_n = diffusion length for electrons

$n_1(p_1)$ = electron (hole) concentration if the electron (hole) fermi level is at the trap energy level.

$n_s(p_s)$ = electron (hole) concentration at the semiconductor surface

Q_f = fixed oxide charges

Q_{sc} = semiconductor charges

Q_{ss} = surface state charges

S_p = surface recombination velocity at the back end of the cell

R = reflection coefficient

qv_p = the difference between majority carrier fermi level and the valence band ($qv_p = kT \ln \frac{N_v}{N_A}$)

v_{th} = thermal velocity

w = depletion width

α = absorption coefficient

$\beta = \frac{q}{kT}$

$\chi_n(\chi_p)$ = effective potential barrier of oxide to electron (hole) tunneling into metal

σ_n = capture cross section area for electrons

τ_t = surface states tunneling time constant

τ_s = tunneling time constant to the metal

ϕ = number of absorbed photons/cm^2.s per unit bandwidth

$q\phi_s$ = difference between the electron and hole quasi fermi levels

ψ_s = band bending of conduction (or valance) bands i.e. the potential difference across the semiconductor

ϕ_m = metal work function

Introduction

A lot of attention has been drawn to MIS contact with ultra thin insulating layer due to their simplicity and their promising applications for solar cells. The physics of MIS structure has been discussed in many papers [1-6]. As applications for the MIS contacts, several models of MIS solar cells have been proposed. A brief review and comments on the most important models are presented below.

Green, et. al. [4,7] proposed a theoretical model which includes both the effects of surface states and tunneling through the oxide layer. Their model has some drawbacks. For the tunneling currents, they only used those from the conduction band and the valence band to metal but they neglected them in the other directions. They used the parameters of thick oxide (oxide permittivity and barrier-height) for the ultra thin oxide layer. They also neglected the effect of interface states on the oxide potential which can change significantly the band bending ψ_s of the conduction and valence bands near the silicon oxide interface.

Following Sze [8], Card and Rhoderick [2,3], and Green et. al. [4], Olson [9] introduced a model which includes the tunneling current, diffusion current, and the light-generated current. But he neglected the effects of the surface states either as recombination centers or as a path between the silicon and the metal through which majority and minority carriers can be transferred. He assumed only depletion region approximation and neglected that inversion or even accumulation conditions can occur depending upon the choice of the metal, the doping, the applied voltage, etc. His model which can be applied only under specific conditions is not a general one. He also assumed that the barrier height of the oxide is fixed (0.5 eV), which is not true because it actually depends on the oxide thickness [10,11]. He also used the permittivity of thick oxide for thin oxide.

Ng and Card [12] proposed another model which includes the tunneling and surface states currents. They neglected the effect of the transition region which generates up to

15% of the generated light current. They also did not use the actual solar spectrum. They neglected the effect of surface states on the band bending. They assumed only an inversion layer in semiconductor, thus, their model is not a general model. They also assumed that the barrier height for minority carriers is equal to $\chi_n = \chi_p = 1.2$ eV. It is not a realistic value.

In this study we have introduced an analytical model which includes the parameters neglected by the above-mentioned authors. The effects of surface states, SiO_2 thickness, substrate doping, fixed oxide charges, and metal work function are all taken into consideration.

2. Theoretical Model.

A complete set of equations is used which includes the hole and electron tunneling currents (J_{pt},J_{nt}) through the oxide layer, the surface states current components (J_{ps},J_{ns} and J_{ss}), the photo current generated in the bulk and in the transition region (J_{Ln} and J_{dr}), the diffusion current (J_{Dn}), and the generation-recombination current in the transition region (J_{rg}). All these current components are shown in Figure 1.

2.1. Band Diagram.

Figure 1 shows the energy band diagram of a MIS (Metal-Silicon dioxide-p type silicon) solar cell. In this diagram it is assumed that the metal is grounded and a positive voltage is applied to the semiconductor, and the cell is under illumination. The fermi levels for electrons and holes are splitted with energy difference equal to $q\phi_s$, the voltage drop across the insulator is Δ, the band bending is ψ_s, the neutral level for the surface states is E_{ss}. The voltage drop across the oxide can be written as:

$$\Delta = E_g + \chi_s - \phi_m - v_p - \psi_s - v \tag{1}$$

From Gauss's law we have

$$\Delta = \frac{d_i}{\epsilon_i}(Q_{sc} + Q_{ss} + Q_F) \tag{2}$$

where Q_F is the fixed oxide charges and is taken to be positive ([9] p. 390). It can be

expressed as

$$Q_F = qN_F \tag{3}$$

Assuming a homogeneous distribution of surface states across the band gap we have

$$Q_{ss} = qD_{it}\,(E_{fn} - E_{fs}) = -q^2 D_{it}(\psi_s + v_p + \phi_s - \phi_o) \tag{4}$$

The semiconductor charges Q_{sc} can be written as [see Appendix A]

$$Q_{sc} = \mp\sqrt{2kT\epsilon_s N_A}\left[\beta\psi_s - e^{-\beta\psi_s} - 1 + \frac{n_i^2}{N_A^2}\left\{e^{\beta\phi_s}\left[e^{\beta\psi_s} - 1\right] - \beta\psi_s\right\}\right]^{1/2} \tag{5}$$

2.2 Band to Band Tunneling Current.

Following Card and Rhoderick [2,3], the hole tunneling current is given by

$$J_{pt} = A_p^* T^2 e^{-\chi_p^{\frac{1}{2}} d_i}\left[e^{-\frac{E_{f_p} - E_{v_o}}{kT}} - e^{-\frac{E_{f_m} - E_{v_o}}{kT}}\right] \tag{6}$$

From Figure 1 we obtain

$$E_{f_p} - E_{v_o} = q(\psi_s + v_q) \tag{7}$$

and

$$E_{f_m} - E_{v_o} = q(\psi_s + v_q + v) \tag{8}$$

Equation (6) can be written as

$$J_{pt} = A_p^* T^2 e^{-\chi_p^{\frac{1}{2}} d_i}\, e^{\beta(\psi_s + v_p)}\left[1 - e^{-\beta v}\right] \tag{9}$$

Similarly, the electron tunneling current can be expressed by

$$J_{nt} = A_n^* T^2 e^{-\chi_n^{\frac{1}{2}} d_i}\left[e^{-\frac{E_{c_o} - E_{fm}}{kT}} - e^{-\frac{E_{c_o} - E_{f_n}}{kT}}\right] \tag{10}$$

From Figure 1 we have

$$E_{c_o} - E_{fm} = E_g - q(\psi_s + v_p + v) \tag{11}$$

and

$$E_{c_o} - E_{fn} = E_g - q(\psi_s + v_p + \phi_s) \tag{12}$$

J_{nt} can be written as

$$J_{nt} = A_n^* T^2 e^{-\chi_n^{\frac{1}{2}} d_i}\, e^{-\frac{E_g}{kT}}\, e^{\beta(\psi_s + v_p)}\left[e^{\beta v} - e^{\beta\phi_s}\right] \tag{13}$$

The values of χ_p and χ_n in (5), (9), (10) and (13) cannot be assumed as those of thick oxide. Assuming $\chi_p = \chi_n = \chi$, we use the curves from Card [10,11] to determine the values of $\chi^{\frac{1}{2}} d_i$.

2.3 Surface States.

Localized states within the forbidden gap at the surface of the semiconductor can affect the performance of the MIS solar cells. The effect of these surface states can be grouped into two categories. The first one is concerned with the electrostatic effect while the second one with the dynamic effect. They are discussed as follows:

a) Electrostatic Effect:

Due to the charge storage in the surface states, the voltage balance in (1) and (2) is affected strongly by the surface states concentration D_{it}. There are two types of surface states, donor-like states and acceptor-like states. The energy of the former is less than E_{ss}, which contributes a positive Q_{ss} when they are emptied while the energy of the latter is greater than E_{ss} which contributes a negative Q_{ss} when they are occupied. The value of Q_{ss} and its sign can increase or decrease the band bending ψ_s. If ψ_s decreases, minority carrier tunneling current J_{nt} decreases and majority carrier tunneling current J_{pt} which contributes to dark current increases. As a result the performance of the solar cell becomes worse. If $q\phi_o = E_{ss} - E_{v_o} \cong \frac{1}{3} Eg$, these effects are adversary for MIS solar cells.

b) Dynamic Effects:

The dynamic effects of the surface states can be explained as follows

i. Surface states provide an additional path for the photo-generated carriers to flow to the metal contact J_{ns} (see Figure 1). This effect enhances the performance of the solar cell due to the increase of the current drawn from the cell.

ii. Surface states provide an additional path for the dark majority carriers J_{ps}.

iii. Surface states act as recombination centers at the surface for the carriers generated inside the semiconductor.

Starting from the equations used by Freeman and Dahlhe [1], all the current components due to the effect of surface states can be calculated (see Appendix B). The electron current through surface states can be expressed as

$$J_{ns} = qD_{it}v_{th}\sigma_n n_i^2 \frac{\tau_s}{\tau_t+\tau_s}\left[\tau_t\sigma_p v_{th}\left[e^{\beta\phi_s}-1\right] + \frac{e^{\beta(\phi_s-v)}-1}{p_1+p_s\, e^{-\beta v}}\right] \qquad (14)$$

The hole current through surface states can be written as

$$J_{ps} = qD_{it}v_{th}\sigma_n n_i^2 \frac{\tau_s}{\tau_t+\tau_s}\left[\tau_t\sigma_p v_{th}\left[e^{\beta\phi_s}-1\right] + \frac{p_s}{n_1}\frac{\sigma_p}{\sigma_n}\frac{1-e^{\beta v}}{(p_1+p_s\, e^{-\beta v})}\right]$$

(15)

and the total current due to surface states is given by

$$\begin{aligned} J_{ss} &= J_{ns} - J_{ps} \\ &= qD_{it}v_{th}\sigma_n n_i^2 \frac{\tau_s}{\tau_t+\tau_s}\frac{1}{p_1+p_s e^{-\beta v}}\left[\left[e^{\beta(\phi_s-v)}-1\right] - \frac{p_s}{n_1}\frac{\sigma_p}{\sigma_n}\left[1-e^{\beta v}\right]\right] \end{aligned} \qquad (16)$$

Equations (14), (15) and (16) are functions of v and ϕ_s, and $\phi_s > v$ all the time. J_{ns} and J_{ps} are, therefore, positive which means that both electrons from conduction band and holes from valence band are captured by surface states and find their ways to the metal. Consequently, both minority carrier current (it enhances the total current drawn from the cell) and majority carrier current (it contributes to dark current) exist. The net effect (J_{ss}) depends on the difference between J_{ns} and J_{ps}.

In our calculations we have found that $J_{ps} > J_{ns}$ except at short circuit conditions (where both J_{ps} and J_{ns} are very small compared to other current components) so the total tunneling current through the surface states deteriorates the performance of the solar cells. The extent of this effect depends on the other parameters used in design of the solar cells.

2.4 Light, Diffusion, and Recombination Currents.

The photo-generated current in the bulk of the semi-conductor is given by (see Appendix C)

$$J_{Ln} = \frac{q\phi\alpha L_n}{\alpha^2 L_n^2 - 1} e^{-\alpha w}\left[\alpha L_n - \frac{F_2(H') - e^{-\alpha H'}\left[\frac{S_n L_n}{D_n} - \alpha L_n\right]}{F_1(H')}\right] \tag{17}$$

The diffusion current is given by (see Appendix C)

$$J_{Dn} = \frac{qD_n}{L_n} n_{p_o} \frac{F_2(H')}{F_1(H')} (e^{\beta\phi_s} - 1) \tag{18}$$

In the depletion region, the electric field is so high that the photo generated carriers are accelerated out of the depletion region before they recombine. This current must be taken into consideration and is written as

$$J_{dr} = q\phi(1 - e^{-\alpha w}) \tag{19}$$

where w, the width of depletion region, is given by

$$w = \sqrt{\frac{2\epsilon_s \psi_s}{qN_A}} \tag{20}$$

Also, the generation recombination current in the depletion region can be written as

$$J_{rg} = \frac{qn_i w}{\tau_n}\left[e^{\frac{1}{2}\beta\psi_s} - 1\right]. \tag{21}$$

2.5 The Total Current and the Balance of Current Components.

Different current components in a MIS solar cell make the device in a non-equilibrium condition, which can be shown by splitting of the Fermi-energy levels of electrons and holes in the semiconductor (see Figure 1). The value of the splitting $q\phi_s$ ($q\phi_s = E_{f_n} - E_{f_p}$) can be determined by balancing the minority-carrier current components in the conduction band

$$J_{L_n} + J_{dr} - J_{rg} - J_{D_n} = J_{ns} + J_{nt} \tag{22}$$

The total current drawn from the cell is given by

$$J_t = J_{ss} + J_{nt} - J_{pt} \tag{23}$$

Rearranging equation (22) we have

$$J_{nt} = J_{Ln} + J_{dr} - J_{rg} - J_{Dn} - J_{ns} \tag{24}$$

Substituting equation (24) into equation (23) and using $J_{ss} = J_{ns} - J_{ps}$ lead to

$$J_t = J_{light} - J_{dark} \tag{25}$$

where

$$J_{light} = J_{Ln} + J_{dr} \tag{26a}$$

and

$$J_{dark} = J_{ps} + J_{pt} + J_{Dn} + J_{rg} \tag{26b}$$

Equation (25) has a similarity with that of the total current of p-n junctions solar cells.

3. Calculations and Results.

The equations in Section 2 have been used to calculate the output parameters of the MIS solar cell. In our calculations we use the actual sunlight spectrum (AM1) which has been obtained from Sze [9] and Hovel [14]. We assume that the back of the cell is not passivated, so the back surface recombination velocity is taken to be $S_p = 10^7$ cm/sec. The density of surface states D_{it} has been found to be between 10^9 - 10^{12} states/cm^2.eV [15], depending on the silicon orientation, the method of oxidation, the oxidation temperature, the annealing, etc. D_{it} also depends on the oxide thickness [16] and on the doping concentration [17].

In this work, the diffusion coefficient is calculated from [18] by the relation

$$D = \frac{D_o}{1 + \left[\frac{N}{10^{17}}\right]^{0.6}} + A_o \tag{27}$$

where $D_o = 35$ cm^2/sec and $A_o = 1.8$ cm^2/sec for p-type semiconductor.

The lifetime τ for good silicon is available in reference [19]. It is found that

$$\tau = \left[28410 + 1.716 \times 10^{-26} N^{1.67}\right]^{-1} \text{ sec.} \tag{28}]$$

for p-type Czochralski (CZ) growth method, and

$$\tau = \left[3330 + 1.716 \times 10^{-26} N^{1.67}\right]^{-1} \text{ sec} \tag{29}$$

for p-type float-zone (FZ) process.

The algorithm used to calculate the open circuit voltage, short circuit current, fill factor, and efficiency is described as follows:

1) Read data

2) Calculate D_n, τ_n and L_n

3) $v = 0$

4) $\phi_s = 0$

5) $\psi_s = 0$

6) Iterate to get ψ_s by using Equation (1) = Equation (2)

7) $J_A = J_{Ln} + J_{dr} - J_{rg} - J_{Dn}$, $J_B = J_{ns} + J_{nt}$

8) If $|J_A - J_B| >$ error, change ϕ_s and go to step 5. Otherwise, calculate J_t.

9) If $v = 0$, $J_{sc} = J_t$

10) Calculate $P = Iv$

11) If P is not maximum, change v and go to step 4. Otherwise save P_{max}

12) Increment v until $J = 0$, then $v_{oc} = v$

13) Calculate efficiency, η, and fill factor FF.

This algorithm is used to study the effects of changing the following parameters on the performance of the MIS solar cells:

a) The metal work function ϕ_m

b) The semiconductor doping N_A

c) The density of surface states D_{it}

d) The fixed oxide charges N_f

e) The cell thickness H

and f) The oxide thickness d_i

When changing one of the previous parameters, the other parameters are taken to be near its optimum values to get maximum efficiency. The values of these parameters are chosen to be $N_A = 2 \times 10^{15} cm^{-3}$, $D_{it} = 5 \times 10^{11}$ states/cm^2.eV, $N_f = 5 \times 10^{11} cm^{-2}$, $\phi_m = 4.1$ eV, $d_i = 20Å$, and $H = 250\mu m$. Other parameters used in our calculation are

listed in Table 1. The values of effective Richardson constants for electrons and holes are discussed by Rhoderick [18], which agree with those values given by Sze and Crowell [9] who used $A_n^* = 112\ A/cm^2.k^2$, and $A_p^* = 32A/cm^2.k^2$. These values are used in our program

Table 1

$n_i = 1.45 \times 10^{10}\ cm^{-3}$

$N_c = 2.8 \times 10^{19} cm^{-3}$

$N_v = 1.04 \times 10^{19} cm^{-3}$

$\sigma_n = \sigma_p = 10^{-15} cm^2$

Eg = 1.12 eV

$v_{th} = 10^7$ cm/sec

$q\phi_o = 1/3\ E_g$.

$x_s = 4.05$ eV

$S_p = 10^7$ cm/sec

$\epsilon_i = 1$

$\tau_o = 10^{-13}$ sec

3.1 Effects of Changing ϕ_m.

The effect of choosing metals with different work functions ϕ_m is shown in Figure 2. For lower ϕ_m we get higher efficiency, and by increasing ϕ_m the efficiency decreases until it reaches near zero. We see that there is a critical metal work function (we call it ϕ_{mc}) after which the efficiency starts decreasing. This can be explained below. For the chosen substrate doping ($N_A = 2 \times 10^{15} cm^{-3}$), the Fermi potential ϕ_F is equal to 0.33 v ($\phi_F = V_T \ln \frac{N_A}{n_i}$). For strong inversion, the band bending ψ_s must satisfy the relation $\psi_s > 2\phi_F$ under dark conditions. Our calculations show that for $\phi_m = 4.3$ V we have $\psi_s = 0.67$ V under zero applied voltage, which corresponds to the onset of the strong inversion. In this case we have $\phi_{mc} = 4.3$V. For $\phi_m < \phi_{mc}$ the semiconductor is strongly

inverted. For $\phi_m > \phi_{mc}$ it is not strongly inverted and the semiconductor charges Q_{sc} is mainly the depletion layer charges.

When the cell is put under illumination, the incident photons generate electron-hole pairs. The electrons go to the surface. When the surface is initially strongly inverted, the concentration of electrons at the surface is not affected too much by the light and the thermal equilibrium can be assumed. But when the surface is not initially in strong inversion, the photo- generated electrons accumulate at the surface and create an optically inverted layer, and the semiconductor charges Q_{sc} increases. This means that a non-equilibrium condition is found and the electron and hole fermi levels (E_{f_n} and E_{f_p}) split. As ϕ_m increases, the surface condition changes from weak inversion to depletion (without light). Therefore, $\phi_s(q\phi_s = E_{f_n} - E_{f_p})$ increases as shown in Figure 3. In this figure we see that for $\phi_m < \phi_{mc}$ ($\phi_{mc} \cong 4.3V$), $\phi_s \cong 0$. But as ϕ_m exceeds ϕ_{mc}, the split ϕ_s increase rapidly with increasing ϕ_m. Therefore, Figure 2 shows that until $\phi_m \cong \phi_{mc}$, the short circuit current J_{sc}, the open circuit voltage v_{oc}, the efficiency η, and the fill factor FF are kept constant but they decrease rapidly when $\phi_m > \phi_{mc}$.

As pointed out earlier, the current drawn from the cell can be written as $J_t = J_{light} - J_{dark}$ (Eq. (25)) and $J_{dark} = J_{ps} + J_{pt} + J_{Dn} + J_{rg}$ (Eq. (26b)). In these equations, J_{rg} and J_{Dn} are functions of ϕ_s, J_{pt} is a function of ψ_s and v, and J_{ps} is a function of ϕ_s and v. For short circuit conditions, an increase in ϕ_m increases ϕ_s, which results in the increase of current. Also from equations (25), (15), and (18), increasing the applied voltage v increases the dark current J_{dark} until the open circuit condition is reached. For $\phi_m < \phi_{mc}$, ϕ_s is approximately equal to the applied voltage and J_{ps} is small. The main component of the dark current is J_{Dn} and the open circuit conditions occur when $J_{Dn} \approx J_{light}$. This leads to higher v_{oc}, FF and η. For $\phi_m > \phi_{mc}$, ϕ_s becomes greater than the applied voltage v_1, so J_{pt}, J_{rg}, J_{Dn}, and J_{ps} increase but J_{ps} becomes the dominant current component (minority carriers n_{p_o} in equation (18) decreases as ϕ_m increases). i.e., the tunneling through surface states becomes the dominant factor affecting

the performance of the MIS devices. The open circuit condition occurs when $J_{ps} \cong J_{light}$. It occurs at lower applied voltage v_{oc} (because $V < \phi_s$). Increasing ϕ_m, raises ϕ_s which increases J_{ps}. As a consequence v_{oc} and efficiency η, decrease and the system goes deeper into nonequilibrium and, hence, the fill factor decreases.

For MIS solar cells, there are no such things which are called minority and majority carrier devices based on variation of metal work function ϕ_m. The reason is that the extracted current from the MIS solar cells is mainly from the minority carriers due to the existence of an inversion layer (either optically induced for $\phi_m > \phi_{mc}$, or thermally exist for $\phi_m < \phi_{mc}$). The differentiation between minority and majority carrier devices is only good for the analysis of MIS structures under dark conditions.

3.2 Effect of Changing N_A.

The dependence of efficiency, open circuit voltage,short circuit current, and fill factor on base doping N_A is shown in Figure 4. The figure demonstrates that for lightly doped substrate, the efficiency is low. By increasing N_A the efficiency, the open circuit voltage, and the fill factor increase until they reach the peaks for the range $N_A = 10^{15}$ -10^{16} cm^{-3}. Then, they start decreasing again. For the short circuit current, it decreases while the doping is increased because the life time of minority carriers decreases with increasing N_A. Using a certain metal work function, the band bending ψ_s increases with increasing N_A due to the increase of metal-semiconductor work function difference until a certain doping density ($N_A = 10^{15}$-10^{16} cm^{-3}) is reached which is called N_{AC}. For $N_A < N_{AC}$ the efficiency is increased due to the increase of ψ_s, or the increase of barrier height. In this case, the semiconductor is thermally inverted and equilibrium conditions occur. For $N_A > N_{AC}$ the semiconductor charges decrease until the surface states charges prevail, which lead to a decrease in ψ_s until the inversion layer vanishes. But due to the optically induced minority carriers an inversion layer is formed which means that the device is in non-equilibrium condition and electron and hole fermi levels

split, i.e., $q\phi_s = E_{fn}-E_{fp}$, increases with increasing $N_A > N_{AC}$. For the similar reason like that for higher $\phi_m > \phi_{mc}$, the open circuit voltage, efficiency and fill factor become lower.

3.3 Effects of changing D_{it}.

The effects of the surface states density D_{it} depend mainly on the choice of the other parameters (ϕ_m,N_A,N_f,d_i,etc). For choosing nearly optimum parameters,we get an inverted semiconductor surface. Increasing the surface states density D_{it} decreases the band bending due to the negative charges in the acceptor-like surface states (see Figure 1), which causes an increase in the potential difference across the insulator, and to a decrease in ψ_s. This reduction of ψ_s will increase the dark component J_{pt} and decrease the minority carrier tunneling current J_{nt}. When D_{it} exceeds a certain level which is called D_{itc}, the effect of surface states as recombination centers disturb the near equilibrium conditions. The hole recombination current through the surface states J_{ps} increases significantly. As a result, $\phi_s(q\phi_s = E_{f_n}-E_{f_p})$ increases rapidly with increasing D_{it} and the dark current increases also substantially. Therefore, the efficiency, the fill factor, and the open circuit voltage decrease as shown in Figure 5. As D_{it} increases further, the recombination current through surface states J_{ps} becomes very large even at short circuit conditions. So, the total current of the device at short circuit J_{sc} decreases. For good quality semiconductor and using hydrogen annealing, the surface states density is of the range 10^{10}-10^{11} states/cm^2eV, and their effect on the performance of the MIS solar cells is reduced if the other parameters (ϕ_m,N_A,N_f,d_i) are well chosen as seen from Figure 5.

3.4 Effects of Changing N_f.

The fixed oxide charges N_f locate inside the oxide in a narrow region next to the Si-$Si0_2$ interface. They are generally positive charges with density in the range 10^{10}-$10^{12}cm^{-2}$. Their concentration depends on silicon orientation and oxidation conditions. They do not change with surface potential and only have electrostatic effect.

They do not have dynamic effect because they do not interact with tunneling carriers. For the thin insulating layer used in MIS solar cells, we can assume that they are located at the Si-$Si0_2$ interface. Because of N_f, the band bending ψ_s increases while the dark majority carrier currents J_{pt} and J_{ps} decrease. As a result, the open circuit voltage and the efficiency of the cell increase as shown in Figure 6. Since N_f does not disturb the near equilibrium conditions, the fill factor does not change with increasing N_f. N_f has a good effect on the metal-insulator-p type semiconductor solar cells, but it causes a decrease in efficiency for a metal-insulator-n type semiconductor cells

3.5 Effect of Changing H.

For very short base of MIS solar cell ($H < 50\mu m$) the number of photo generated carriers are very small, so, the short circuit current is small. Since $H << L_n$ (the diffusion length) there is also less recombination which means higher open circuit voltage. As the thickness H increases, the short circuit current increases and the open circuit voltage decreases. Since the former has greater effect on efficiency than that of the latter, the efficiency increases. The effect of cell thickness on the fill factor is negligible for the whole range of H, which is shown in Figure 7, because changing H will not alter the near equilibrium conditions. When $H >> L_n$ the effect of back surface recombination can be neglected so the open circuit voltage saturates. Approximately all incident light is absorbed in the first part of the base next to the oxide, so the short circuit current is also saturated. Therefore, both the efficiency and the fill factor saturate.

In our model we have neglected the effect of base resistivity and assumed zero voltage drop across the neutral region of the base. Taking these effects into consideration the efficiency will decrease as $H >> L_n$ for long base.

3.5 Effects of changing d_i.

The oxide thickness is the most critical parameter which affects the performance of the MIS solar cells. For thinner oxide, the hole tunneling becomes easier which means that the dark current becomes larger. The total current becomes smaller and the open circuit

voltage is reduced and the efficiency decreases. As the thickness of the oxide layer increases, the hole tunneling through the insulator decreases which leads to a decrease in dark current. So the efficiency and open circuit voltage increases until a certain thickness of oxide d_{ic} is reached. For $d_i > d_{ic}$, the electron tunneling becomes more difficult and higher concentration of photogenerated electrons exists in semiconductor which creates an optically induced inversion layer and the split between electron and hole fermi levels increases, so the dark current increases again which causes a decrease in the open circuit voltage and efficiency. When $d_i > d_{ic}$ and d_i reaches a certain value, the dark current becomes very large even at short circuit conditions and the total current becomes very small (J_{sc} decreases rapidly and reaches approximately to zero) as shown in Figure 8.

4. Conclusion.

Our comprehensive analytical model shows that none of the parameters of a MIS solar cell can dominate. Therefore, all the current components (J_{pt},J_{nt},J_{ps},J_{ns},J_{ss},J_{Dn}, J_{dr},J_{rg}) must be included as we do in our model. This work has emphasized the importance of assuming a non-equilibrium condition because when the device becomes under equilibrium, only specific values of solar cell parameters can be used. Besides, we have used the actual values of permittivity ϵ_i and barrier heights χ_p and χ_n for a more realistic modeling for the MIS solar cells.

Acknowledgment

This work was partially supported by NASA/MSFC grants. One of the authors (F. D. Ho) would like to express his sincere thanks to Mr. Teddy M. Edge and Mr. Michael D. Martin, The NASA Marshall Space Flight Center, for the discussions of some technical problems.

APPENDIX A

Semiconductor Charges (Q_{sc})

To calculate Q_{sc} we have to solve Poisson's equation

$$\frac{d^2\psi}{dx^2} = -\frac{q}{\epsilon_s}(p-n-N_A) \tag{A-1}$$

where

$$p = N_A\, e^{-\beta\psi} \tag{A-2}$$

$$n = \frac{n_i^2}{N_A}\, e^{\beta(\psi+\phi_s)} \tag{A-3}$$

We have assumed that a non-equilibrium condition exists in semiconductor. This is a realistic assumption due to light generated minority carriers and due to the voltage drop across the cell. Also, it is assumed that the minority carrier quasi-fermi level is constant through the transition region, which means that the separation between the two fermi levels is independent of x and equal to that at the surface. This is shown in Figure 1. Substituting equations (A-2) and (A-3) in equation (A-1), integrating, and using the relation

$$E(x) = -\frac{d\psi}{dx} \tag{A-4}$$

we can find the electric field. The semiconductor charges Q_{sc} can be written as

$$Q_{sc} = -\epsilon_s\, E_{surface} \tag{A-5}$$

so

$$Q_{sc} = \mp\sqrt{2kT\epsilon_s N_A}\left[\beta\psi_s - e^{-\beta\psi_s} - 1 + \frac{n_i^2}{N_A^2}\left\{e^{\beta\phi_s}(e^{\beta\psi_s}-1) - \beta\psi_s\right\}\right]^{1/2} \tag{A-6}$$

This relation is a more general relation. Many papers assumed initially that the semiconductor is in depletion [8] and used the depletion layer approximation to calculate Q_{sc}

$$Q_{sc} = -\sqrt{2\epsilon_s q N_A}\,\psi_s^{1/2} \qquad \text{(A-7)}$$

But the semiconductor may be at inversion, depletion or accumulation. For high efficiency MIS solar cells, the surface of the semiconductor must be inverted initially before exposing the cell to light. Some other authors [6] calculated Q_{sc} assuming equilibrium condition so they got an expression for Q_{sc} like equation (A-6) but without the term $e^{\beta\phi_s}$:

$$Q_{sc} = \mp\sqrt{2kT\epsilon_s N_A}\left[\beta\psi_s - e^{-\beta\psi_s} - 1 + \frac{n_i^2}{N_A^2}\left\{e^{\beta\psi_s} - 1 - \beta\psi_s\right\}\right]^{1/2} \qquad \text{(A-8)}$$

To see the effect of the term $e^{\beta\phi_s}$ we compare (A-6) with (A-8). In our calculations we have calculated the solar cell parameters for two different values of fixed oxide charges N_f. We choose $d_i = 25\text{Å}$ for the onset of non-equilibrium conditions. The results are shown in Table 2. From the table we see that for $N_f = 0$, the efficiency is much smaller for non-equilibrium equation (A-6) than that for equilibrium equation (A-8). The reason is that for equation (A-8) the surface becomes near strong inversion but for equation (A-6) the surface becomes weakly inverted at short circuit conditions with higher value of ϕ_s. Therefore, as the semiconductor surface deviates from equilibrium, the fill factor drops sharply and the efficiency decreases. For $N_f = 5.10^{11}\text{cm}^{-2}$, the surface is initially inverted for both equations (A-6) and (A-8). The split between the two fermi levels becomes small and near equilibrium conditions occur. In this case, there is not much difference between calculations with equation (A-8) or with equation (A-6). Since the system is not in exact equilibrium ($\phi_s \neq 0$), calculations with (A-6) give sightly lower efficiency than that with (A-8) as is shown in Table 2.

TABLE 2

EQUATION	N_f (cm^{-2})	ψ_s (V)	ϕ_s (V)	η (%)	FF (10^{-2})	V_{oc} (mV)	J_{sc} (mA/cm^2)	
(A–8)	0	0.627	0.136	11.32	61.81	510	35.7	equilibrium
(A–6)	0	0.456	0.309	7.466	39.13	506	37.7	nonequilibrium
(A–8)	5.10^{11}	0.745	0.029	15.1	80.25	524	35.92	equilibrium
(A–6)	5.10^{11}	0.676	0.09	14.67	68.91	565	37.7	nonequilibrium

Calculation was made for $N_A = 2.10^{15} cm^{-3}$, $D_{it} = 55 \times 10^{11} cm^{-2} eV^{-1}$

$\phi_m = 4.1$ V, H = 2.50 μm, $\delta = 25A^\circ$

APPENDIX B

Current Components Due to Surface States

Following the approach of Freeman and Dahlke [1], the electron current from the conduction band to the surface states is given by

$$J_{ns} = qD_{it}v_{th}\sigma_n\left[(1-f_t)n_s - f_t n_1\right] \tag{B-1}$$

The hole current from the valence band to the surface states can be written as

$$J_{ps} = qD_{it}v_{th}\sigma_p\left[f_t p_s - (1-f_t)p_1\right] \tag{B-2}$$

and the total current through the surface states is

$$J_{ss} = J_{ns} - J_{ps} = \frac{qD_{it}}{\tau_t}\left[f_t - f_m\right] \tag{B-3}$$

In the above equations

$$n_1 = N_c e^{\frac{E_{ss}-E_{co}}{kT}} = N_c e^{-\frac{Eg-q\phi_o}{kT}} \tag{B-4}$$

$$p_1 = N_v e^{-\frac{E_{ss}-E_{vo}}{kT}} = N_v e^{-\beta\phi_o} \tag{B-5}$$

$$n_s = N_c e^{\frac{E_{fn}-E_{co}}{kT}} = \frac{n_i^2}{N_A} e^{\beta(\psi_s+\phi_s)} \tag{B-6}$$

$$p_s = N_v e^{-\frac{E_{fp}-E_{vo}}{kT}} = N_A e^{-\beta\psi_s} \tag{B-7}$$

$$f_t = \frac{\tau_t\ f_{to} + \tau_s\ f_m}{\tau_t + \tau_s} \tag{B-8}$$

$$f_{t_o} = \frac{n_s\sigma_n + p_1\sigma_p}{(n_s+n_1)\sigma_n + (p_s+p_1)\sigma_p} \tag{B-9}$$

$$\tau_t = \tau_o e^{\chi^{\frac{1}{2}}d_i} \tag{B-10}$$

$$\tau_s = \frac{1}{v_{th}[\sigma_n(n_s+n_1)+\sigma_p(p_s+p_1)]} \tag{B-11}$$

and

$$f_m = \frac{1}{1 + \exp\left[\frac{E_s-E_{fm}}{kT}\right]} = \frac{1}{1 + \frac{p_s}{p_1} e^{-\beta v}} \tag{B-12}$$

Substituting equations (B-4) through (B-12) into equations (B-1), (B-2) and (B-3), respectively, we obtain equations (14), (15), and (16), respectively.

APPENDIX C

The Photogeneration and Diffusion Currents

Using Hovel's approach [14] for p-n junction solar cells, we can calculate the photo-generated current and the diffusion current for MIS solar cells by solving the continuity equation

$$D_n \frac{d^2(n_p - n_{p_o})}{dx^2} + G(\lambda,x) - \frac{n_p - n_{p_o}}{\tau_n} = 0 \qquad (C\text{-}1)$$

Where $G(\lambda,x)$ is the generation rate of electron-hole pairs at distance x from the semiconductor surface for the incident light with wavelength λ.

$$G(\lambda,x) = \alpha(\lambda)\phi(\lambda)e^{-\alpha x} \qquad (C\text{-}2)$$

Where $\alpha(\lambda)$ is the absorption coefficient and $\phi(\lambda)$ is the number of absorbed photons/cm^2.s per unit bandwidth which is given by

$$\phi(\lambda) = F_o(\lambda)[1 - R(\lambda)] \qquad (C\text{-}3)$$

where $F_o(\lambda)$ is the number of incident photons/cm^2.s per unit bandwidths and $R(\lambda)$ is the reflection coefficient. The following boundary conditions are used:

a) at $x = w$

$$n_p - n_{p_o} = n_s e^{-\beta\psi_s} - n_{p_o} = n_{p_o}(e^{\beta\phi_s} - 1) \qquad (C\text{-}4)$$

b) at $x = H$

$$D_n \frac{d}{dx}(n_p - n_{p_o}) = - S_p(n_p - n_{p_o}) \qquad (C\text{-}5)$$

Solving equation (C-1) we get

$$n_p - n_{p_o} = \frac{\alpha\phi\tau_n}{\alpha^2 L_n^2 - 1} e^{-\alpha w}\left[\cosh\frac{x-w}{L_n} - e^{-\alpha(x-w)} + \left[\frac{s_n L_n}{D_n} - \alpha L_n\right]\frac{e^{-\alpha H'}}{F_1(H')} - \frac{F_2(H')}{F_1(H')}\sinh\frac{x-w}{L_n}\right]$$
$$+ n_{p_o}(e^{\beta\phi_s} - 1)\frac{F_2(H-x)}{F_1(H')} \qquad (C\text{-}6)$$

where

$$H' = H - w \tag{C-7}$$

$$F_1(y) = \frac{s_n L_n}{D_n} \sinh \frac{y}{L_n} + \cosh \frac{y}{L_n} \tag{C-8}$$

$$F_2(y) = \frac{s_n L_n}{D_n} \cosh \frac{y}{L_n} + \sinh \frac{y}{L_n} \tag{C-9}$$

The current can be written as

$$J_n = qD_n \left[\frac{dn_p}{dx}\right]_{x=w} = J_{Ln} - J_{Dn} \tag{C-10}$$

where J_{Ln} is the photogenerated current in the bulk which is given by

$$J_{Ln} = \frac{q\phi\alpha L_n}{\alpha^2 L_n^2 - 1} e^{-\alpha w}\left[\alpha L_n - \frac{F_2(H') - e^{-\alpha H'}\left[\frac{s_n L_n}{D_n} - \alpha L_n\right]}{F_1(H')}\right] \tag{C-11}$$

and J_{Dn} is the diffusion current which can be written as

$$J_{Dn} = \frac{qD_n}{L_n} n_{p_o} (e^{\beta\phi_s} - 1) \frac{F_2(H')}{F_1(H')} \tag{C-12}$$

References

1. Freeman and Dahlke, "Theory of Tunneling into Interface States," Solid State Electronics, Vol. 13, pp. 1483-1503, 1970.
2. H. C. Card and E. H. Rhoderick, "Studies of Tunnel MOS Diodes I. Interface Effects on Silicon Schottky Diodes," J. Phys. D: Appl. Phys., Vol. 4, pp. 1589-1601, 1971.
3. H. C. Card and E. H. Rhoderick, "Studies of Tunnel MOS Diodes II. Thermal Equilibrium Considerations," J. Phys. D. Appl. Phys., Vol. 4, pp. 1602-1611, 1970.
4. M. A. Green, F. D. King and J. Shewchun, "Minority Carrier MIS Tunnel Diodes and their Application to Electron- and Photo-Voltage Energy Conversion - I, Theory," Solid State Electronics, Vol. 17, pp. 551-561, 1974.
5. P. Chattopadhyay and A. N. Daw, "On the Current Transport Mechanism in a MIS Diode," Solid State Electronics, Vol. 29, pp. 555-560, 1986.
6. P. Chattopadhyay and A. N. Daw, "Effect of Surface States on the Barrier Height in a MIS Diode in the Presence of Inversion," International Journal of Electronics, Vol. 58, No. 5, pp. 775-779, 1985.
7. J. Shewchun, R. Singh, And M. A. Green, "Theory of Metal-Iinsulator-Semiconductor Solar Cells,", J. Appl. Phys, Vol. 48, No. 2. 1977.
8. Larry C. Olsen, "Model Calculations for Metal-Insulator-Semiconductor Solar Cell," Solid State Electronics, Vol. 20, pp. 741-751, 1977.
9. S. M. Sze, "Physics of Semiconductor Devices," J. Wiley & Sons, 1981.
10. H. C. Card, "Photo-Voltage Properties of MIS - Schottky Barriers," Solid State Electronics, Vol. 20, pp. 971-976, 1977.
11. K. K. Ng and H. C. Card, "Asymmetry in the $Si0_2$ Tunneling Barriers to Electrons and Holes," J. Appl. Phys. 51(4), pp. 2153, 1980.

12. K. K. Ng and H. C. Card, "A Comparison of Majority- and Minority- Carrier Silicon MIS Solar Cells," IEEE Trans. on Electron Devices, Vol. ED 27, pp. 716-724, 1980.

13. A. A. Abdou and S. E. D. Habib, "Optically Induced Inversion in MIS Solar Cells," Solid State Electronics, Vol. 29, pp. 751-758, 1986.

14. H. J. Hovel, "Semiconductors and Semimetals, Vol. 11: Solar Cells, Academic Press, 1975.

15. P. Antognetti, D. Antomidis, R. Dutton and W. Wolham (editors), "Process and Device Simulation for MOS-VLSI Circuits," NATO Series, Series E: Applied Sciences, No. 62, 1983.

16. H. C. Card, "Si-SiO_2 Interface State Spectroscopy Using MOS Tunneling Structures," Solid State Electronics, Vol. 22, pp. 809-817, 1979.

17. J. Snel, "The Doped Si/SiO_2 Interface," Solid States Electronics, Vol. 24, pp. 135-139, 1981.

18. E. H. Rhoderick, "Metal-Semiconductor Contacts," Clarendon Press, Oxford, 1978.

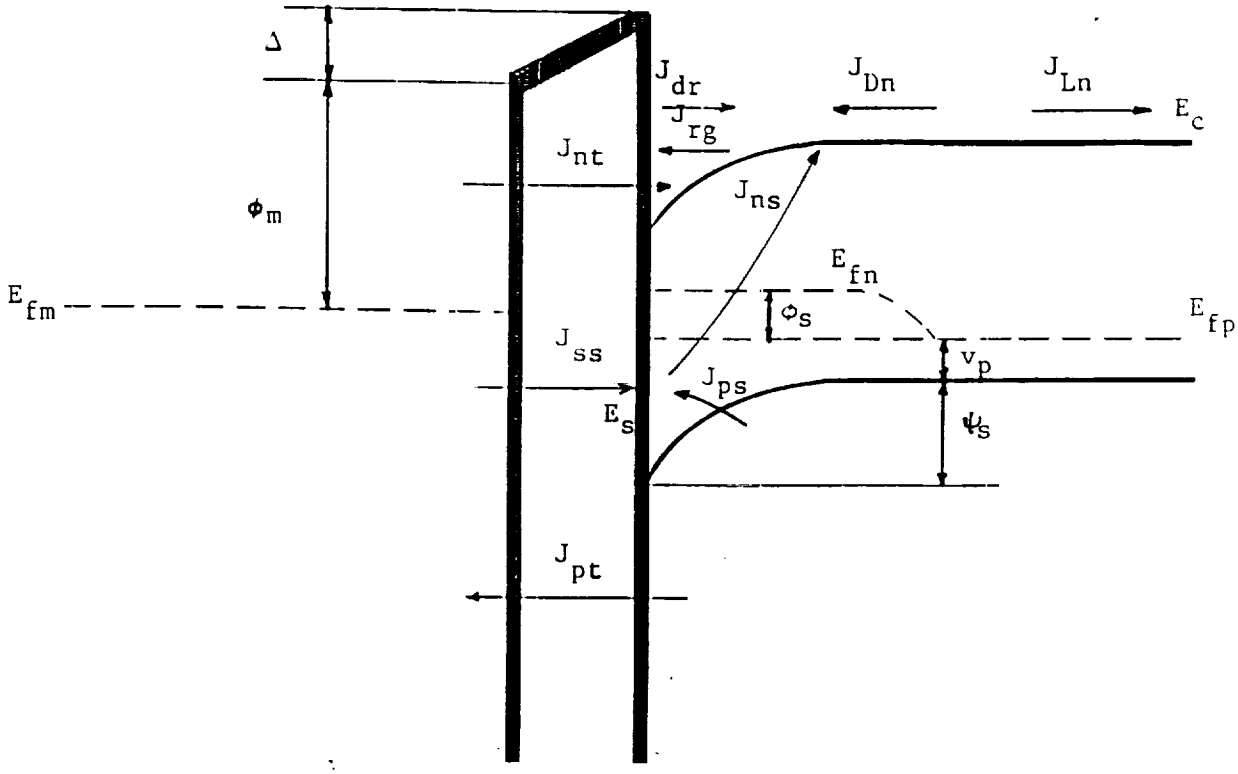

Figure 1: Energy band diagram for the MIS p-type solar cell.

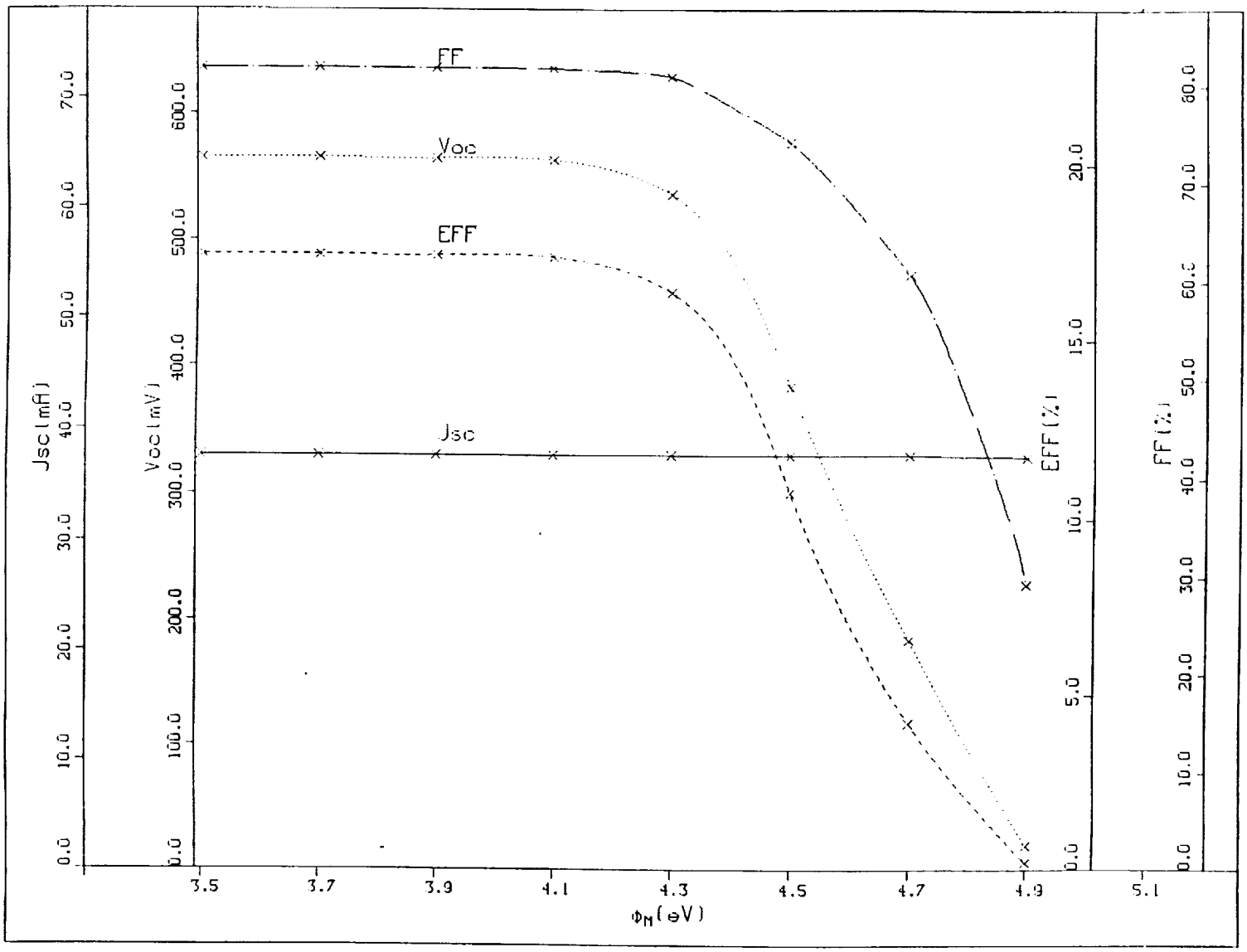

Figure 2: The efficiency Eff, the open circuit voltage v_{oc}, the short circuit current J_{sc}, and the fill factor FF versus the metal work function ϕ_m for the MIS solar cell.

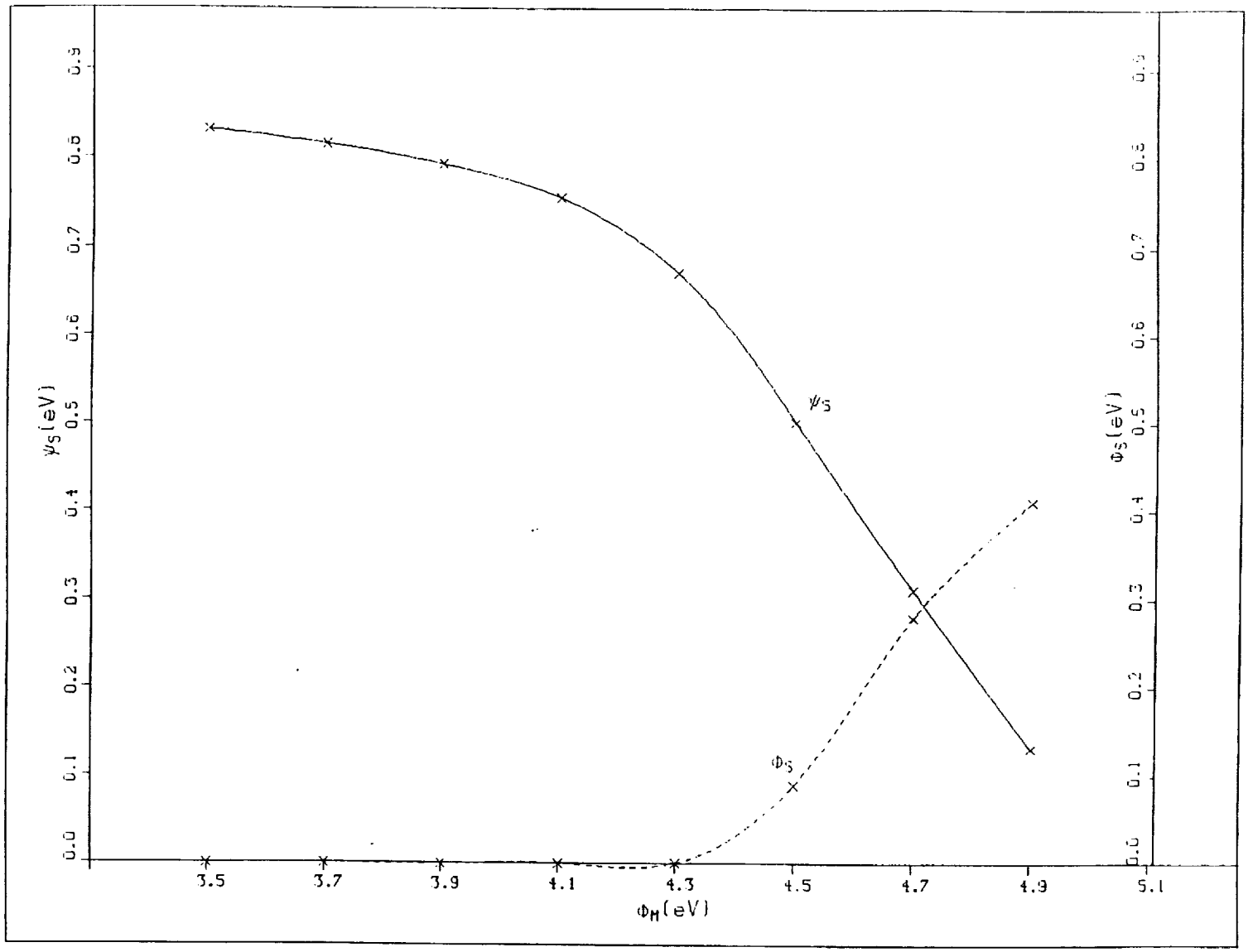

Figure 3: Variations of the surface potential ψ_s and the split between the two fermi levels of electrons and holes ϕ_s as functions of ϕ_m.

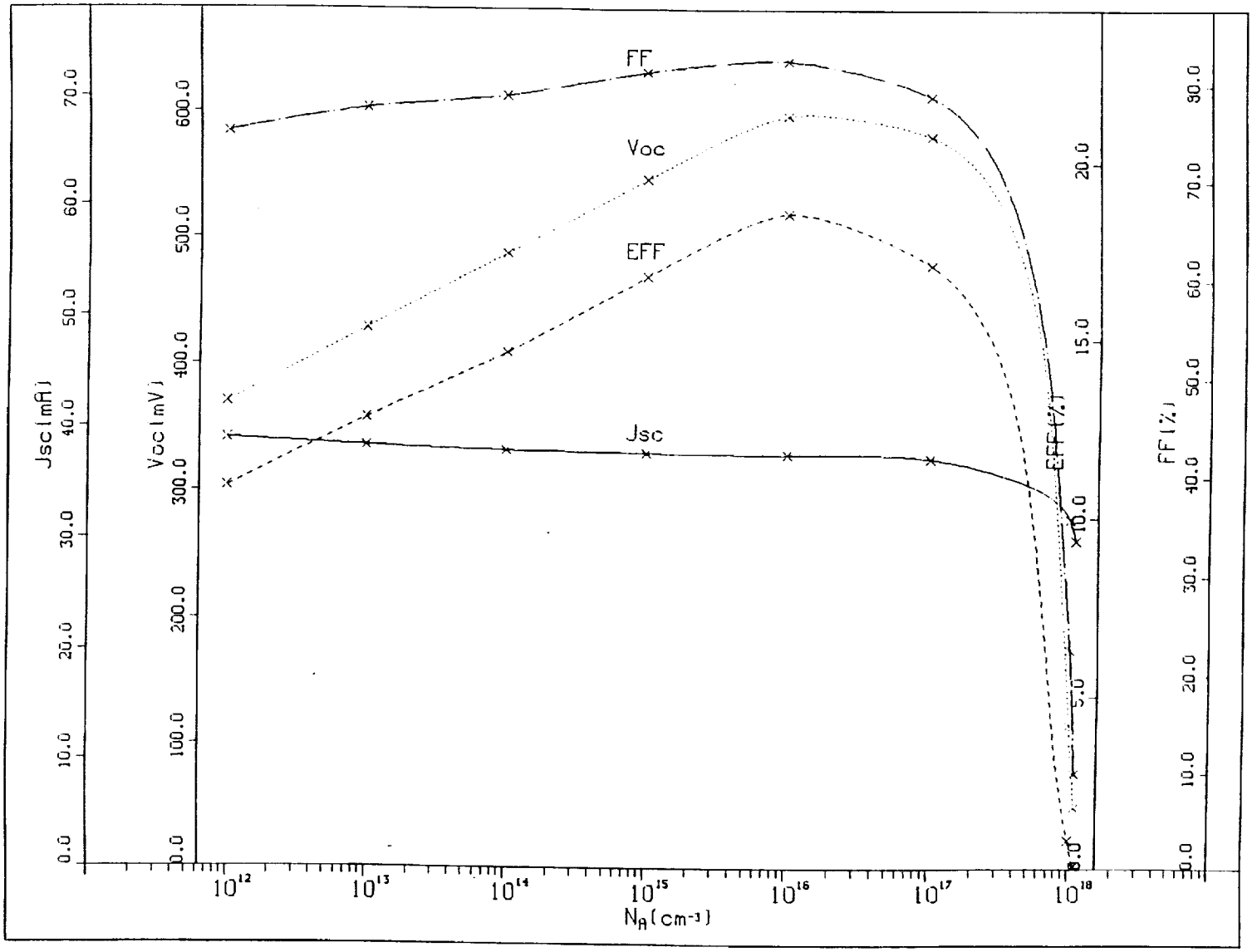

Figure 4: Eff, v_{oc}, J_{sc}, and FF versus the silicon doping density N_A for the MIS cell.

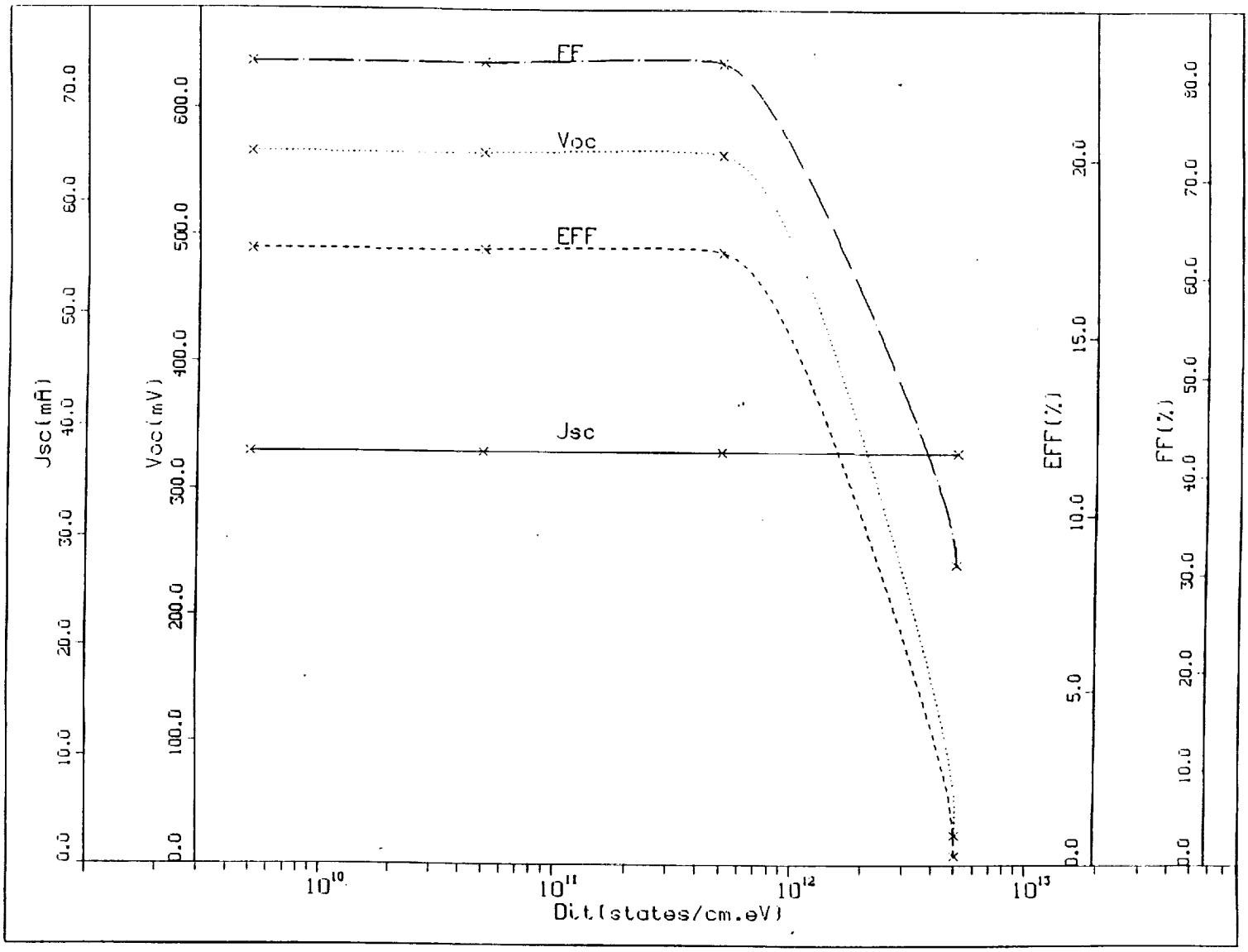

Figure 5: Eff, v_{oc}, J_{sc}, and FF versus the surface states density D_{it}.

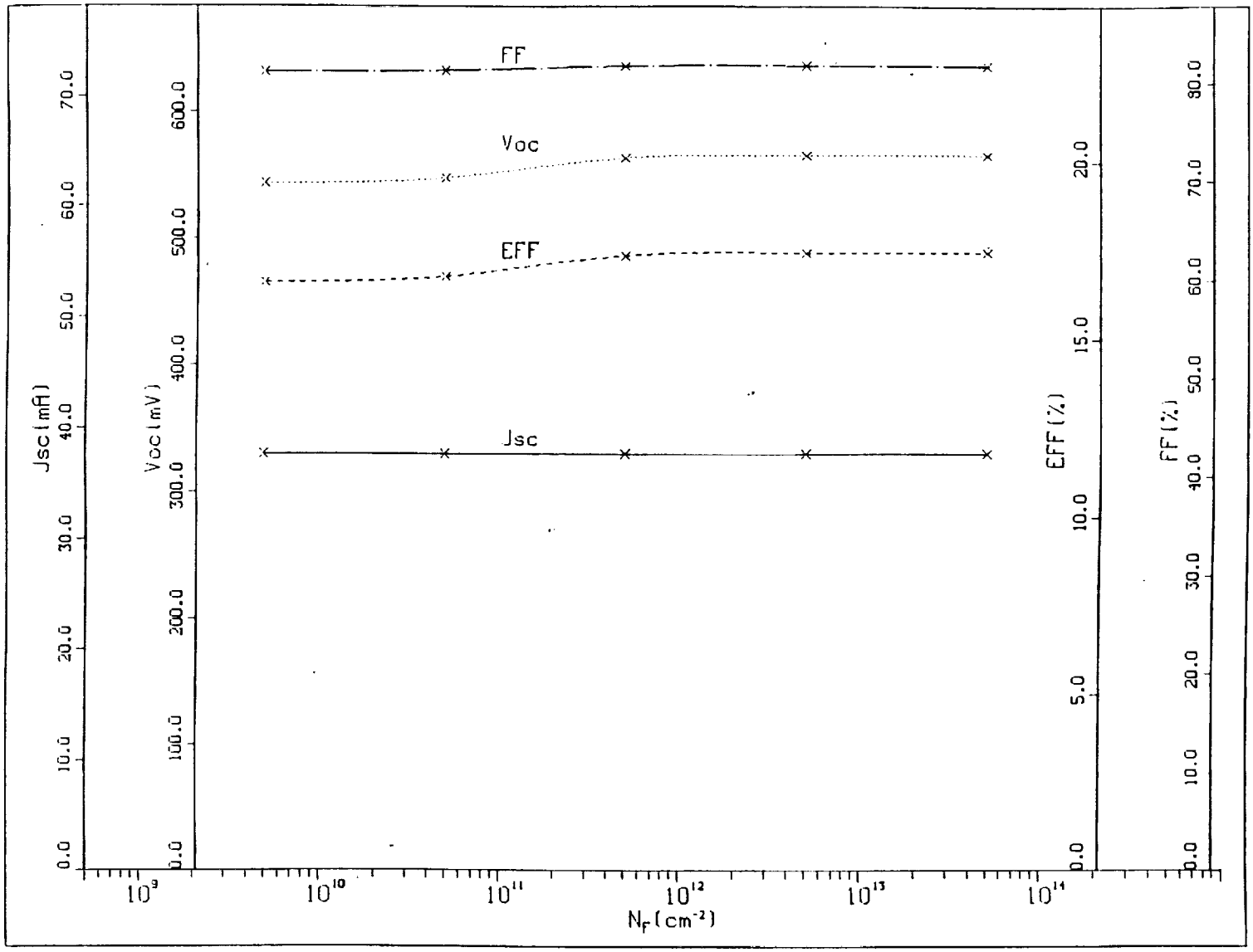

Figure 6. Eff, v_{oc}, J_{sc}, and FF versus the fixed oxide charges N_f.

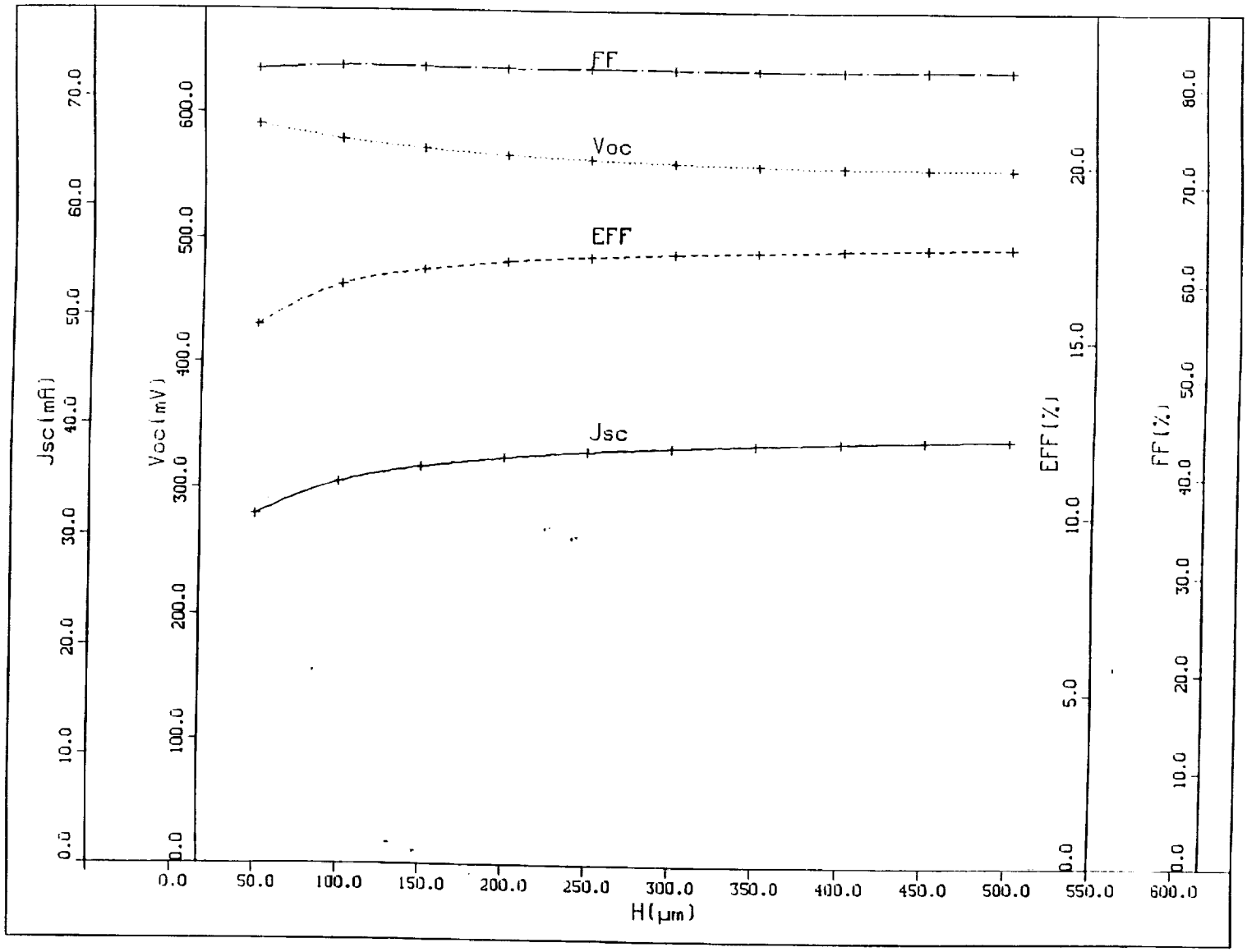

Figure 7. Eff, v_{oc}, J_{sc}, and FF versus the cell thickness H.

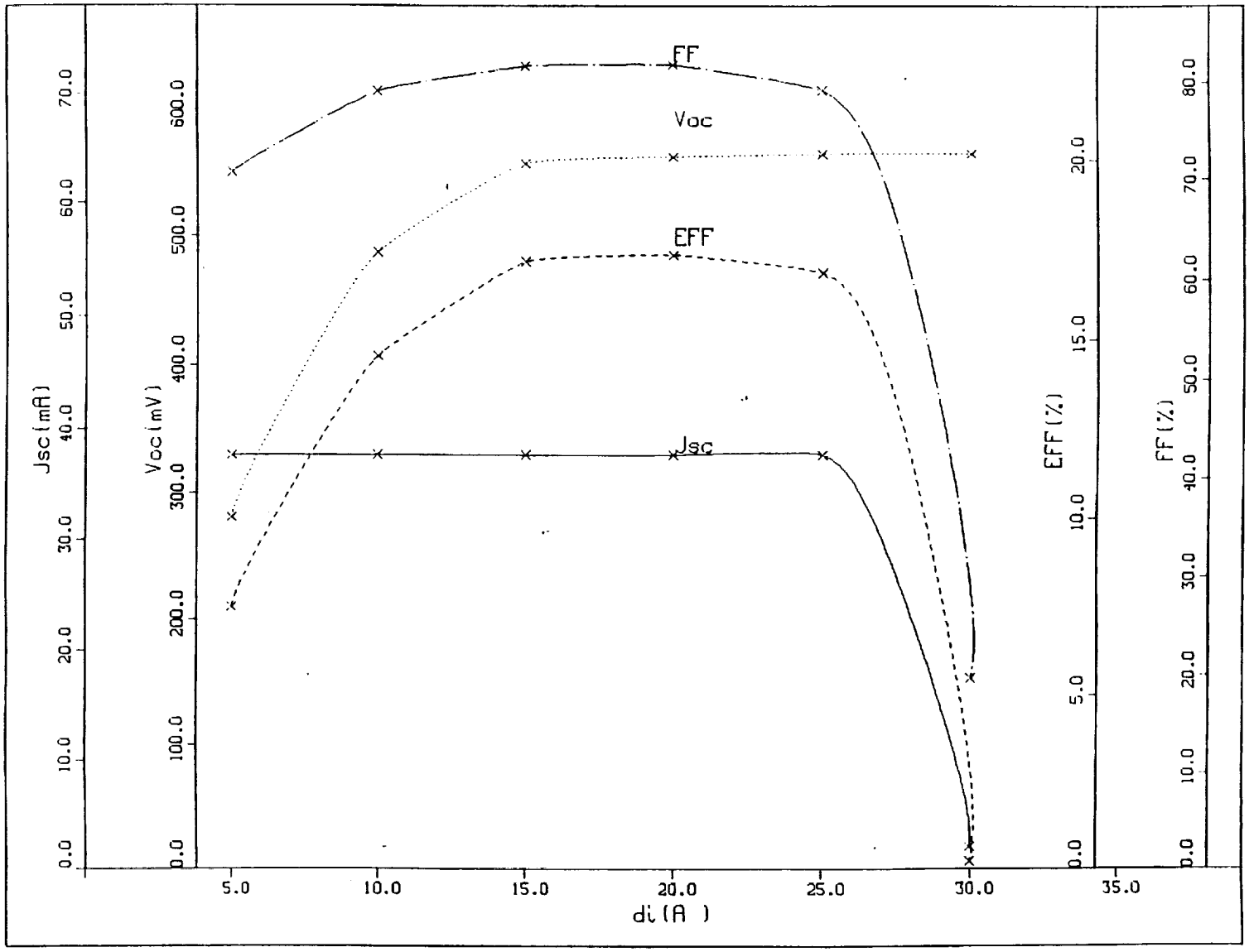

Figure 8. Eff, v_{oc}, J_{sc}, and FF versus the oxide thickness d_i.

APPENDIX B

Data Used in Figures 4–12

ELECTROSTATIC POTENTIAL DISTRIBUTION - IL SOLAR CELL

TERMINAL VOLTAGE = .30 V
UNIT IN VOLT

HOR-uM / VER-uM	25.00	25.02	25.27	26.02	38.52	63.52	88.52	113.52	146.02
0.00	0.30	0.40	0.44	0.45	0.45	0.45	0.45	0.45	0.45
0.05	0.25	0.30	0.37	0.37	0.37	0.37	0.37	0.37	0.37
0.10	0.21	0.24	0.31	0.31	0.31	0.31	0.31	0.31	0.31
0.15	0.18	0.19	0.25	0.26	0.26	0.26	0.26	0.26	0.26
0.20	0.15	0.16	0.21	0.22	0.22	0.21	0.21	0.21	0.21
0.25	0.13	0.14	0.17	0.18	0.18	0.17	0.17	0.17	0.17
0.30	0.11	0.11	0.13	0.13	0.13	0.13	0.13	0.12	0.12
0.37	0.09	0.09	0.10	0.10	0.09	0.09	0.09	0.08	0.08
0.47	0.07	0.07	0.08	0.08	0.08	0.07	0.06	0.06	0.06
0.60	0.05	0.05	0.05	0.06	0.06	0.05	0.05	0.05	0.05
0.75	0.03	0.03	0.03	0.04	0.04	0.03	0.03	0.03	0.03
0.92	0.02	0.02	0.02	0.02	0.02	0.02	0.02	0.02	0.02
1.12	0.01	0.01	0.01	0.01	0.01	0.01	0.01	0.01	0.01
1.35	0.00	0.00	0.00	0.00	0.00	0.00	0.00	0.00	0.00
1.60	0.00	0.00	0.00	0.00	0.00	0.00	0.00	0.00	0.00
1.87	0.00	0.00	0.00	0.00	0.00	0.00	0.00	0.00	0.00
2.17	0.00	0.00	0.00	0.00	0.00	0.00	0.00	0.00	0.00
2.55	0.00	0.00	0.00	0.00	0.00	0.00	0.00	0.00	0.00
3.05	-0.00	-0.00	-0.00	-0.00	-0.00	-0.00	-0.00	-0.00	-0.00
3.80	-0.00	-0.00	-0.00	-0.00	-0.00	-0.00	-0.00	-0.00	-0.00
4.80	-0.00	-0.00	-0.00	-0.00	-0.00	-0.00	-0.00	-0.00	-0.00
6.30	-0.00	-0.00	-0.00	-0.00	-0.00	-0.00	-0.00	-0.00	-0.00
8.30	-0.00	-0.00	-0.00	-0.00	-0.00	-0.00	-0.00	-0.00	-0.00
10.80	-0.00	-0.00	-0.00	-0.00	-0.00	-0.00	-0.00	-0.00	-0.00
14.55	-0.00	-0.00	-0.00	-0.00	-0.00	-0.00	-0.00	-0.00	-0.00
19.55	-0.00	-0.00	-0.00	-0.00	-0.00	-0.00	-0.00	-0.00	-0.00
27.05	-0.00	-0.00	-0.00	-0.00	-0.00	-0.00	-0.00	-0.00	-0.00
37.05	-0.00	-0.00	-0.00	-0.00	-0.00	-0.00	-0.00	-0.00	-0.00
52.05	-0.00	-0.00	-0.00	-0.00	-0.00	-0.00	-0.00	-0.00	-0.00
72.05	-0.00	-0.00	-0.00	-0.00	-0.00	-0.00	-0.00	-0.00	-0.00
94.55	-0.00	-0.00	-0.00	-0.00	-0.00	-0.00	-0.00	-0.00	-0.00
117.05	-0.00	-0.00	-0.00	-0.00	-0.00	-0.00	-0.00	-0.00	-0.00
137.05	-0.00	-0.00	-0.00	-0.00	-0.00	-0.00	-0.00	-0.00	-0.00
154.55	-0.00	-0.00	-0.00	-0.00	-0.00	-0.00	-0.00	-0.00	-0.00
169.55	-0.00	-0.00	-0.00	-0.00	-0.00	-0.00	-0.00	-0.00	-0.00
182.05	-0.00	-0.00	-0.00	-0.00	-0.00	-0.00	-0.00	-0.00	-0.00
189.55	-0.00	-0.00	-0.00	-0.00	-0.00	-0.00	-0.00	-0.00	-0.00
194.55	-0.00	-0.00	-0.00	-0.00	-0.00	-0.00	-0.00	-0.00	-0.00
197.05	-0.00	-0.00	-0.00	-0.00	-0.00	-0.00	-0.00	-0.00	-0.00
199.30	-0.00	-0.00	-0.00	-0.00	-0.00	-0.00	-0.00	-0.00	-0.00
201.05	-0.00	-0.00	-0.00	-0.00	-0.00	-0.00	-0.00	-0.00	-0.00
202.30	-0.00	-0.00	-0.00	-0.00	-0.00	-0.00	-0.00	-0.00	-0.00
203.05	-0.00	-0.00	-0.00	-0.00	-0.00	-0.00	-0.00	-0.00	-0.00
203.55	0.00	0.00	0.00	0.00	0.00	0.00	0.00	0.00	0.00
203.80	0.00	0.00	0.00	0.00	0.00	0.00	0.00	0.00	0.00

ELECTRON CONCENTRATION - IL SOLAR CELL

TERMINAL VOLTAGE= 0.30 V
UNIT IN ELECTRONS PER CUBIC CM

HOR-uM / VER-uM	25.00	25.02	25.27	26.02	38.52	63.52	88.52	113.52	146.02
0.00	1.4E+10	7.9E+15	3.8E+16	4.7E+16	4.7E+16	4.8E+16	4.9E+16	5.0E+16	5.0E+16
0.05	1.6E+14	1.2E+14	1.9E+15	2.5E+15	2.5E+15	2.5E+15	2.5E+15	2.5E+15	2.5E+15
0.10	1.0E+13	2.4E+12	1.1E+14	1.8E+14	1.8E+14	1.7E+14	1.7E+14	1.6E+14	1.6E+14
0.15	9.5E+11	1.1E+11	4.5E+12	8.6E+12	8.2E+12	7.4E+12	6.9E+12	6.5E+12	6.3E+12
0.20	1.3E+11	1.1E+10	1.8E+11	3.6E+11	3.4E+11	2.9E+11	2.6E+11	2.4E+11	2.3E+11
0.25	2.9E+10	1.8E+09	1.2E+10	2.2E+10	2.0E+10	1.6E+10	1.4E+10	1.2E+10	1.2E+10
0.30	6.1E+09	3.2E+08	4.9E+08	7.4E+08	6.4E+08	4.9E+08	3.9E+08	3.4E+08	3.1E+08
0.37	1.5E+09	8.4E+07	4.3E+07	4.6E+07	3.8E+07	2.7E+07	2.0E+07	1.7E+07	1.5E+07
0.47	3.3E+08	1.9E+07	1.1E+07	1.3E+07	1.0E+07	7.0E+06	5.0E+06	4.0E+06	3.6E+06
0.60	6.8E+07	4.4E+06	2.6E+06	3.5E+06	3.0E+06	2.4E+06	1.9E+06	1.7E+06	1.6E+06
0.75	1.8E+07	1.4E+06	8.0E+05	1.0E+06	9.5E+05	8.6E+05	7.9E+05	7.4E+05	7.2E+05
0.92	6.9E+06	7.0E+05	4.1E+05	4.5E+05	4.4E+05	4.4E+05	4.3E+05	4.3E+05	4.2E+05
1.12	4.1E+06	6.0E+05	3.5E+05	3.4E+05	3.4E+05	3.5E+05	3.5E+05	3.6E+05	3.6E+05
1.35	3.5E+06	7.1E+05	4.3E+05	3.9E+05	3.9E+05	4.0E+05	4.1E+05	4.1E+05	4.2E+05
1.60	3.7E+06	9.7E+05	6.0E+05	5.4E+05	5.3E+05	5.4E+05	5.6E+05	5.6E+05	5.7E+05
1.87	4.2E+06	1.4E+06	8.9E+05	7.9E+05	7.8E+05	7.9E+05	8.1E+05	8.2E+05	8.2E+05
2.17	5.0E+06	2.0E+06	1.3E+06	1.2E+06	1.2E+06	1.2E+06	1.2E+06	1.2E+06	1.2E+06
2.55	6.2E+06	3.1E+06	2.1E+06	1.8E+06	1.8E+06	1.8E+06	1.8E+06	1.9E+06	1.9E+06
3.05	8.3E+06	5.0E+06	3.4E+06	3.0E+06	3.0E+06	3.0E+06	3.0E+06	3.0E+06	3.1E+06
3.80	1.2E+07	8.3E+06	5.9E+06	5.3E+06	5.2E+06	5.2E+06	5.2E+06	5.2E+06	5.2E+06
4.80	1.8E+07	1.5E+07	1.1E+07	9.6E+06	9.4E+06	9.4E+06	9.5E+06	9.5E+06	9.5E+06
6.30	2.9E+07	2.6E+07	2.0E+07	1.8E+07	1.8E+07	1.8E+07	1.8E+07	1.8E+07	1.8E+07
8.30	4.9E+07	4.7E+07	3.8E+07	3.5E+07	3.4E+07	3.4E+07	3.4E+07	3.4E+07	3.4E+07
10.30	8.5E+07	8.4E+07	7.3E+07	6.6E+07	6.4E+07	6.4E+07	6.5E+07	6.5E+07	6.5E+07
14.55	1.6E+08	1.6E+08	1.4E+08	1.3E+08	1.3E+08	1.3E+08	1.3E+08	1.3E+08	1.3E+08
19.55	2.9E+08	2.9E+08	2.8E+08	2.6E+08	2.5E+08	2.5E+08	2.5E+08	2.5E+08	2.5E+08
27.05	5.6E+08	5.6E+08	5.5E+08	5.2E+08	5.1E+08	5.1E+08	5.1E+08	5.1E+08	5.1E+08
37.05	1.1E+09	1.1E+09	1.1E+09	1.1E+09	1.1E+09	1.1E+09	1.1E+09	1.1E+09	1.0E+09
52.05	2.0E+09	2.0E+09	1.9E+09	1.9E+09	1.9E+09	1.9E+09	1.9E+09	1.9E+09	1.9E+09
72.05	3.2E+09	3.2E+09	3.2E+09	3.2E+09	3.1E+09	3.1E+09	3.1E+09	3.1E+09	3.1E+09
94.55	4.4E+09	4.4E+09	4.4E+09	4.4E+09	4.3E+09	4.3E+09	4.3E+09	4.3E+09	4.3E+09
117.05	5.2E+09	5.2E+09	5.2E+09	5.1E+09	5.0E+09	5.0E+09	5.0E+09	5.0E+09	5.0E+09
137.05	5.2E+09	5.2E+09	5.2E+09	5.2E+09	5.1E+09	5.1E+09	5.1E+09	5.1E+09	5.1E+09
154.55	4.7E+09	4.7E+09	4.7E+09	4.7E+09	4.6E+09	4.6E+09	4.6E+09	4.6E+09	4.6E+09
169.55	3.6E+09	3.6E+09	3.6E+09	3.6E+09	3.5E+09	3.5E+09	3.5E+09	3.5E+09	3.5E+09
182.05	2.7E+09	2.7E+09	2.7E+09	2.7E+09	2.6E+09	2.6E+09	2.6E+09	2.6E+09	2.6E+09
189.55	1.9E+09	1.9E+09	1.9E+09	1.9E+09	1.9E+09	1.8E+09	1.8E+09	1.8E+09	1.8E+09
194.55	1.4E+09	1.4E+09	1.4E+09	1.4E+09	1.4E+09	1.4E+09	1.4E+09	1.4E+09	1.4E+09
197.05	9.9E+08	9.9E+08	9.9E+08	9.9E+08	9.7E+08	9.7E+08	9.7E+08	9.7E+08	9.7E+08
199.30	6.2E+08	6.2E+08	6.2E+08	6.2E+08	6.1E+08	6.1E+08	6.1E+08	6.1E+08	6.1E+08
201.05	3.5E+08	3.5E+08	3.4E+08	3.4E+08	3.4E+08	3.4E+08	3.4E+08	3.4E+08	3.4E+08
202.30	1.7E+08	1.7E+08	1.7E+08	1.7E+08	1.7E+08	1.7E+08	1.7E+08	1.7E+08	1.7E+08
203.05	5.9E+07	5.9E+07	5.9E+07	5.8E+07	5.7E+07	5.7E+07	5.7E+07	5.7E+07	5.7E+07
203.55	1.2E+05	1.2E+05	1.2E+05	1.2E+05	1.2E+05	1.2E+05	1.2E+05	1.2E+05	1.2E+05

HOLE CONCENTRATION DISTRIBUTION - IL SOLAR CELL

TERMINAL VOLTAGE= 0.30 V

HOR-uM / VER-uM	25.00	25.02	25.27	26.02	38.52	63.52	88.52	113.52	146.02
0.00	1.5E+10	1.7E+04	2.2E+02	9.2E+01	7.0E+01	4.7E+01	3.4E+01	2.7E+01	2.5E+01
0.05	4.8E+11	1.6E+08	3.3E+05	1.3E+05	9.7E+04	6.7E+04	4.9E+04	4.1E+04	3.7E+04
0.10	3.5E+12	2.5E+10	4.5E+07	1.4E+07	1.1E+07	8.2E+06	6.3E+06	5.3E+06	4.9E+06
0.15	2.0E+13	8.7E+11	2.9E+09	8.8E+08	7.2E+08	5.4E+08	4.3E+08	3.7E+08	3.4E+08
0.20	9.1E+13	1.2E+13	1.0E+11	3.1E+10	2.6E+10	2.1E+10	1.7E+10	1.5E+10	1.4E+10
0.25	3.1E+14	8.0E+13	2.0E+12	6.6E+11	5.6E+11	4.6E+11	3.9E+11	3.6E+11	3.4E+11
0.30	1.0E+15	5.1E+14	5.5E+13	2.3E+13	2.0E+13	1.8E+13	1.6E+13	1.5E+13	1.4E+13
0.37	1.7E+15	1.7E+15	7.1E+14	4.1E+14	3.8E+14	3.5E+14	3.3E+14	3.2E+14	3.1E+14
0.47	1.7E+15	1.7E+15	1.7E+15	1.7E+15	1.5E+15	1.5E+15	1.4E+15	1.4E+15	1.3E+15
0.60	1.7E+15	1.7E+15	1.7E+15	1.7E+15	1.7E+15	1.7E+15	1.7E+15	1.7E+15	1.7E+15
0.75	1.7E+15	1.7E+15	1.7E+15	1.7E+15	1.7E+15	1.7E+15	1.7E+15	1.7E+15	1.7E+15
0.92	1.7E+15	1.7E+15	1.7E+15	1.7E+15	1.7E+15	1.7E+15	1.7E+15	1.7E+15	1.7E+15
1.12	1.7E+15	1.7E+15	1.7E+15	1.7E+15	1.7E+15	1.7E+15	1.7E+15	1.7E+15	1.7E+15
1.35	1.7E+15	1.7E+15	1.7E+15	1.7E+15	1.7E+15	1.7E+15	1.7E+15	1.7E+15	1.7E+15
1.60	1.7E+15	1.7E+15	1.7E+15	1.7E+15	1.7E+15	1.7E+15	1.7E+15	1.7E+15	1.7E+15
1.87	1.7E+15	1.7E+15	1.7E+15	1.7E+15	1.7E+15	1.7E+15	1.7E+15	1.7E+15	1.7E+15
2.17	1.7E+15	1.7E+15	1.7E+15	1.7E+15	1.7E+15	1.7E+15	1.7E+15	1.7E+15	1.7E+15
2.55	1.7E+15	1.7E+15	1.7E+15	1.7E+15	1.7E+15	1.7E+15	1.7E+15	1.7E+15	1.7E+15
3.05	1.7E+15	1.7E+15	1.7E+15	1.7E+15	1.7E+15	1.7E+15	1.7E+15	1.7E+15	1.7E+15
3.80	1.7E+15	1.7E+15	1.7E+15	1.7E+15	1.7E+15	1.7E+15	1.7E+15	1.7E+15	1.7E+15
4.80	1.7E+15	1.7E+15	1.7E+15	1.7E+15	1.7E+15	1.7E+15	1.7E+15	1.7E+15	1.7E+15
6.30	1.7E+15	1.7E+15	1.7E+15	1.7E+15	1.7E+15	1.7E+15	1.7E+15	1.7E+15	1.7E+15
8.30	1.7E+15	1.7E+15	1.7E+15	1.7E+15	1.7E+15	1.7E+15	1.7E+15	1.7E+15	1.7E+15
10.80	1.7E+15	1.7E+15	1.7E+15	1.7E+15	1.7E+15	1.7E+15	1.7E+15	1.7E+15	1.7E+15
14.55	1.7E+15	1.7E+15	1.7E+15	1.7E+15	1.7E+15	1.7E+15	1.7E+15	1.7E+15	1.7E+15
19.55	1.7E+15	1.7E+15	1.7E+15	1.7E+15	1.7E+15	1.7E+15	1.7E+15	1.7E+15	1.7E+15
27.05	1.7E+15	1.7E+15	1.7E+15	1.7E+15	1.7E+15	1.7E+15	1.7E+15	1.7E+15	1.7E+15
37.05	1.7E+15	1.7E+15	1.7E+15	1.7E+15	1.7E+15	1.7E+15	1.7E+15	1.7E+15	1.7E+15
52.05	1.7E+15	1.7E+15	1.7E+15	1.7E+15	1.7E+15	1.7E+15	1.7E+15	1.7E+15	1.7E+15
72.05	1.7E+15	1.7E+15	1.7E+15	1.7E+15	1.7E+15	1.7E+15	1.7E+15	1.7E+15	1.7E+15
94.55	1.7E+15	1.7E+15	1.7E+15	1.7E+15	1.7E+15	1.7E+15	1.7E+15	1.7E+15	1.7E+15
117.05	1.7E+15	1.7E+15	1.7E+15	1.7E+15	1.7E+15	1.7E+15	1.7E+15	1.7E+15	1.7E+15
137.05	1.7E+15	1.7E+15	1.7E+15	1.7E+15	1.7E+15	1.7E+15	1.7E+15	1.7E+15	1.7E+15
154.55	1.7E+15	1.7E+15	1.7E+15	1.7E+15	1.7E+15	1.7E+15	1.7E+15	1.7E+15	1.7E+15
169.55	1.7E+15	1.7E+15	1.7E+15	1.7E+15	1.7E+15	1.7E+15	1.7E+15	1.7E+15	1.7E+15
182.05	1.7E+15	1.7E+15	1.7E+15	1.7E+15	1.7E+15	1.7E+15	1.7E+15	1.7E+15	1.7E+15
189.55	1.7E+15	1.7E+15	1.7E+15	1.7E+15	1.7E+15	1.7E+15	1.7E+15	1.7E+15	1.7E+15
194.55	1.7E+15	1.7E+15	1.7E+15	1.7E+15	1.7E+15	1.7E+15	1.7E+15	1.7E+15	1.7E+15
197.05	1.7E+15	1.7E+15	1.7E+15	1.7E+15	1.7E+15	1.7E+15	1.7E+15	1.7E+15	1.7E+15
199.80	1.7E+15	1.7E+15	1.7E+15	1.7E+15	1.7E+15	1.7E+15	1.7E+15	1.7E+15	1.7E+15
201.05	1.7E+15	1.7E+15	1.7E+15	1.7E+15	1.7E+15	1.7E+15	1.7E+15	1.7E+15	1.7E+15
202.30	1.7E+15	1.7E+15	1.7E+15	1.7E+15	1.7E+15	1.7E+15	1.7E+15	1.7E+15	1.7E+15
203.05	1.7E+15	1.7E+15	1.7E+15	1.7E+15	1.7E+15	1.7E+15	1.7E+15	1.7E+15	1.7E+15
203.55	1.7E+15	1.7E+15	1.7E+15	1.7E+15	1.7E+15	1.7E+15	1.7E+15	1.7E+15	1.7E+15

ELECTROSTATIC POTENTIAL DISTRIBUTION - IL SOLAR CELL

TERMINAL VOLTAGE = .40 V
UNIT IN VOLT

HOR-uM / VER-uM	25.00	25.02	25.27	26.02	38.52	63.52	88.52	113.52	146.02
0.00	0.40	0.47	0.50	0.50	0.48	0.46	0.46	0.46	0.45
0.05	0.34	0.37	0.42	0.42	0.40	0.39	0.38	0.38	0.38
0.10	0.29	0.31	0.35	0.36	0.34	0.33	0.32	0.32	0.32
0.15	0.25	0.25	0.30	0.30	0.29	0.27	0.27	0.26	0.26
0.20	0.21	0.21	0.25	0.25	0.24	0.23	0.22	0.22	0.22
0.25	0.18	0.18	0.20	0.21	0.20	0.19	0.18	0.18	0.18
0.30	0.14	0.14	0.15	0.16	0.15	0.14	0.13	0.13	0.13
0.37	0.11	0.11	0.11	0.11	0.10	0.09	0.09	0.09	0.09
0.47	0.09	0.09	0.09	0.08	0.08	0.07	0.07	0.07	0.06
0.60	0.06	0.06	0.06	0.06	0.06	0.06	0.05	0.05	0.05
0.75	0.04	0.04	0.04	0.04	0.04	0.04	0.03	0.03	0.03
0.92	0.02	0.02	0.02	0.02	0.02	0.02	0.02	0.02	0.02
1.12	0.01	0.01	0.01	0.01	0.01	0.01	0.01	0.01	0.01
1.35	0.00	0.00	0.00	0.00	0.00	0.00	0.00	0.00	0.00
1.60	0.00	0.00	0.00	0.00	0.00	0.00	0.00	0.00	0.00
1.87	0.00	0.00	0.00	0.00	0.00	0.00	0.00	0.00	0.00
2.17	-0.00	-0.00	-0.00	-0.00	-0.00	-0.00	-0.00	-0.00	-0.00
2.55	-0.00	-0.00	-0.00	-0.00	-0.00	-0.00	-0.00	-0.00	-0.00
3.05	-0.00	-0.00	-0.00	-0.00	-0.00	-0.00	-0.00	-0.00	-0.00
3.80	-0.00	-0.00	-0.00	-0.00	-0.00	-0.00	-0.00	-0.00	-0.00
4.80	-0.00	-0.00	-0.00	-0.00	-0.00	-0.00	-0.00	-0.00	-0.00
6.30	-0.00	-0.00	-0.00	-0.00	-0.00	-0.00	-0.00	-0.00	-0.00
8.30	-0.00	-0.00	-0.00	-0.00	-0.00	-0.00	-0.00	-0.00	-0.00
10.80	-0.00	-0.00	-0.00	-0.00	-0.00	-0.00	-0.00	-0.00	-0.00
14.55	-0.00	-0.00	-0.00	-0.00	-0.00	-0.00	-0.00	-0.00	-0.00
19.55	-0.00	-0.00	-0.00	-0.00	-0.00	-0.00	-0.00	-0.00	-0.00
27.05	-0.00	-0.00	-0.00	-0.00	-0.00	-0.00	-0.00	-0.00	-0.00
37.05	-0.00	-0.00	-0.00	-0.00	-0.00	-0.00	-0.00	-0.00	-0.00
52.05	-0.00	-0.00	-0.00	-0.00	-0.00	-0.00	-0.00	-0.00	-0.00
72.05	-0.00	-0.00	-0.00	-0.00	-0.00	-0.00	-0.00	-0.00	-0.00
94.55	-0.00	-0.00	-0.00	-0.00	-0.00	-0.00	-0.00	-0.00	-0.00
117.05	-0.00	-0.00	-0.00	-0.00	-0.00	-0.00	-0.00	-0.00	-0.00
137.05	-0.00	-0.00	-0.00	-0.00	-0.00	-0.00	-0.00	-0.00	-0.00
154.55	-0.00	-0.00	-0.00	-0.00	-0.00	-0.00	-0.00	-0.00	-0.00
169.55	-0.00	-0.00	-0.00	-0.00	-0.00	-0.00	-0.00	-0.00	-0.00
182.05	-0.00	-0.00	-0.00	-0.00	-0.00	-0.00	-0.00	-0.00	-0.00
189.55	-0.00	-0.00	-0.00	-0.00	-0.00	-0.00	-0.00	-0.00	-0.00
194.55	-0.00	-0.00	-0.00	-0.00	-0.00	-0.00	-0.00	-0.00	-0.00
197.05	-0.00	-0.00	-0.00	-0.00	-0.00	-0.00	-0.00	-0.00	-0.00
199.30	-0.00	-0.00	-0.00	-0.00	-0.00	-0.00	-0.00	-0.00	-0.00
201.05	-0.00	-0.00	-0.00	-0.00	-0.00	-0.00	-0.00	-0.00	-0.00
202.30	-0.00	-0.00	-0.00	-0.00	-0.00	-0.00	-0.00	-0.00	-0.00
203.05	-0.00	-0.00	-0.00	-0.00	-0.00	-0.00	-0.00	-0.00	-0.00
203.55	0.00	0.00	0.00	0.00	0.00	0.00	0.00	0.00	0.00
203.80	0.00	0.00	0.00	0.00	0.00	0.00	0.00	0.00	0.00

ELECTRON CONCENTRATION - IL SOLAR CELL

TERMINAL VOLTAGE= 0.40 V
UNIT IN ELECTRONS PER CUBIC CM

HOR-uM / VER-uM	25.00	25.02	25.27	26.02	38.52	63.52	88.52	113.52	146.02
0.00	6.5E+11	1.3E+16	3.6E+16	3.8E+16	4.5E+16	6.9E+16	9.2E+16	1.1E+17	1.1E+17
0.05	7.3E+14	5.1E+14	1.7E+15	1.9E+15	2.3E+15	3.6E+15	4.8E+15	5.6E+15	5.8E+15
0.10	1.1E+13	6.1E+13	1.4E+14	1.7E+14	2.1E+14	3.4E+14	4.5E+14	5.2E+14	5.4E+14
0.15	1.6E+13	1.1E+13	1.6E+13	1.9E+13	2.5E+13	4.1E+13	5.4E+13	6.1E+13	6.4E+13
0.20	2.8E+12	2.0E+12	2.2E+12	2.6E+12	3.5E+12	5.5E+12	6.9E+12	7.7E+12	8.0E+12
0.25	4.9E+11	3.5E+11	3.2E+11	3.9E+11	4.8E+11	6.7E+11	8.0E+11	8.5E+11	8.6E+11
0.30	5.3E+10	3.7E+10	2.1E+10	2.3E+10	2.5E+10	3.1E+10	3.4E+10	3.4E+10	3.4E+10
0.37	1.0E+10	7.1E+09	2.9E+09	2.7E+09	2.5E+09	2.5E+09	2.5E+09	2.4E+09	2.3E+09
0.47	3.0E+09	2.7E+09	2.0E+09	1.7E+09	1.6E+09	1.4E+09	1.3E+09	1.2E+09	1.1E+09
0.60	1.1E+09	1.1E+09	1.0E+09	1.1E+09	1.0E+09	1.0E+09	9.5E+08	9.1E+08	8.9E+08
0.75	5.6E+08	5.6E+08	5.7E+08	6.2E+08	6.2E+08	6.3E+08	6.3E+08	6.3E+08	6.3E+08
0.92	4.3E+08	4.3E+08	4.4E+08	4.6E+08	4.7E+08	4.8E+08	4.9E+08	5.0E+08	5.1E+08
1.12	4.7E+08	4.7E+08	4.7E+08	4.7E+08	4.8E+08	5.0E+08	5.2E+08	5.3E+08	5.3E+08
1.35	6.5E+08	6.5E+08	6.4E+08	6.4E+08	6.5E+08	6.7E+08	6.9E+08	7.0E+08	7.1E+08
1.60	1.0E+09	9.9E+08	9.8E+08	9.7E+08	9.8E+08	1.0E+09	1.0E+09	1.0E+09	1.0E+09
1.87	1.5E+09	1.5E+09	1.5E+09	1.5E+09	1.5E+09	1.5E+09	1.6E+09	1.6E+09	1.6E+09
2.17	2.4E+09	2.4E+09	2.3E+09	2.3E+09	2.3E+09	2.4E+09	2.4E+09	2.4E+09	2.4E+09
2.55	3.7E+09	3.7E+09	3.7E+09	3.7E+09	3.7E+09	3.7E+09	3.8E+09	3.8E+09	3.8E+09
3.05	6.3E+09	6.3E+09	6.2E+09	6.2E+09	6.2E+09	6.2E+09	6.3E+09	6.3E+09	6.3E+09
3.80	1.1E+10	1.1E+10	1.1E+10	1.1E+10	1.1E+10	1.1E+10	1.1E+10	1.1E+10	1.1E+10
4.80	2.0E+10	2.0E+10	2.0E+10	2.0E+10	2.0E+10	2.0E+10	2.0E+10	2.0E+10	2.0E+10
6.30	3.8E+10	3.8E+10	3.8E+10	3.8E+10	3.8E+10	3.8E+10	3.8E+10	3.8E+10	3.8E+10
8.30	7.2E+10	7.2E+10	7.2E+10	7.2E+10	7.1E+10	7.2E+10	7.2E+10	7.2E+10	7.2E+10
10.80	1.4E+11	1.4E+11	1.4E+11	1.4E+11	1.4E+11	1.4E+11	1.4E+11	1.4E+11	1.4E+11
14.55	2.7E+11	2.7E+11	2.7E+11	2.7E+11	2.7E+11	2.7E+11	2.7E+11	2.7E+11	2.7E+11
19.55	5.3E+11	5.3E+11	5.3E+11	5.3E+11	5.2E+11	5.2E+11	5.3E+11	5.3E+11	5.3E+11
27.05	1.0E+12	1.0E+12	1.0E+12	1.0E+12	1.0E+12	1.0E+12	1.0E+12	1.0E+12	1.0E+12
37.05	1.9E+12	1.9E+12	1.9E+12	1.9E+12	1.9E+12	1.9E+12	1.9E+12	1.9E+12	1.9E+12
52.05	3.4E+12	3.4E+12	3.4E+12	3.4E+12	3.4E+12	3.4E+12	3.4E+12	3.4E+12	3.4E+12
72.05	5.2E+12	5.2E+12	5.2E+12	5.2E+12	5.2E+12	5.2E+12	5.2E+12	5.2E+12	5.2E+12
94.55	6.6E+12	6.6E+12	6.6E+12	6.6E+12	6.6E+12	6.6E+12	6.6E+12	6.6E+12	6.6E+12
117.05	7.2E+12	7.2E+12	7.2E+12	7.2E+12	7.2E+12	7.2E+12	7.2E+12	7.2E+12	7.2E+12
137.05	7.0E+12	7.0E+12	7.0E+12	7.0E+12	7.0E+12	7.0E+12	7.0E+12	7.0E+12	7.0E+12
154.55	5.9E+12	5.9E+12	5.9E+12	5.9E+12	5.9E+12	5.9E+12	5.9E+12	5.9E+12	5.9E+12
169.55	4.4E+12	4.4E+12	4.4E+12	4.4E+12	4.4E+12	4.4E+12	4.4E+12	4.4E+12	4.4E+12
182.05	3.2E+12	3.2E+12	3.2E+12	3.2E+12	3.2E+12	3.2E+12	3.2E+12	3.2E+12	3.2E+12
189.55	2.2E+12	2.2E+12	2.2E+12	2.2E+12	2.2E+12	2.2E+12	2.2E+12	2.2E+12	2.2E+12
194.55	1.7E+12	1.7E+12	1.7E+12	1.7E+12	1.7E+12	1.7E+12	1.7E+12	1.7E+12	1.7E+12
197.05	1.2E+12	1.2E+12	1.2E+12	1.2E+12	1.2E+12	1.2E+12	1.2E+12	1.2E+12	1.2E+12
199.30	7.2E+11	7.2E+11	7.2E+11	7.2E+11	7.3E+11	7.3E+11	7.3E+11	7.3E+11	7.3E+11
201.05	4.0E+11	4.0E+11	4.0E+11	4.0E+11	4.0E+11	4.0E+11	4.0E+11	4.0E+11	4.0E+11
202.30	2.0E+11	2.0E+11	2.0E+11	2.0E+11	2.0E+11	2.0E+11	2.0E+11	2.0E+11	2.0E+11
203.05	6.8E+10	6.8E+10	6.8E+10	6.8E+10	6.8E+10	6.8E+10	6.8E+10	6.8E+10	6.8E+10
203.55	1.2E+05	1.2E+05	1.2E+05	1.2E+05	1.2E+05	1.2E+05	1.2E+05	1.2E+05	1.2E+05

HOLE CONCENTRATION DISTRIBUTION - IL SOLAR CELL

TERMINAL VOLTAGE= 0.40 V

HOR-uM / VER-uM	25.00	25.02	25.27	26.02	38.52	63.52	88.52	113.52	146.02
0.00	3.2E+08	8.4E+01	4.1E+00	2.8E+00	8.0E+00	1.6E+01	1.7E+01	1.7E+01	1.6E+01
0.05	1.7E+10	7.1E+05	7.9E+03	4.7E+03	1.3E+04	2.5E+04	2.8E+04	2.8E+04	2.7E+04
0.10	1.7E+11	1.7E+08	1.5E+06	7.7E+05	1.9E+06	3.5E+06	3.9E+06	3.9E+06	3.8E+06
0.15	1.4E+12	1.1E+10	1.4E+08	6.6E+07	1.5E+08	2.6E+08	2.8E+08	2.8E+08	2.8E+08
0.20	8.6E+12	2.9E+11	6.9E+09	3.3E+09	6.6E+09	1.1E+10	1.2E+10	1.2E+10	1.2E+10
0.25	4.5E+13	4.2E+12	2.0E+11	9.8E+10	1.8E+11	2.7E+11	3.0E+11	3.0E+11	2.9E+11
0.30	3.0E+14	7.9E+13	1.0E+13	5.7E+12	8.9E+12	1.2E+13	1.3E+13	1.3E+13	1.3E+13
0.37	1.3E+15	7.7E+14	3.0E+14	2.1E+14	2.6E+14	3.1E+14	3.2E+14	3.1E+14	3.1E+14
0.47	1.7E+15	1.7E+15	1.7E+15	1.5E+15	1.5E+15	1.5E+15	1.5E+15	1.4E+15	1.4E+15
0.60	1.7E+15	1.7E+15	1.7E+15	1.7E+15	1.7E+15	1.7E+15	1.7E+15	1.7E+15	1.7E+15
0.75	1.7E+15	1.7E+15	1.7E+15	1.7E+15	1.7E+15	1.7E+15	1.7E+15	1.7E+15	1.7E+15
0.92	1.7E+15	1.7E+15	1.7E+15	1.7E+15	1.7E+15	1.7E+15	1.7E+15	1.7E+15	1.7E+15
1.12	1.7E+15	1.7E+15	1.7E+15	1.7E+15	1.7E+15	1.7E+15	1.7E+15	1.7E+15	1.7E+15
1.35	1.7E+15	1.7E+15	1.7E+15	1.7E+15	1.7E+15	1.7E+15	1.7E+15	1.7E+15	1.7E+15
1.60	1.7E+15	1.7E+15	1.7E+15	1.7E+15	1.7E+15	1.7E+15	1.7E+15	1.7E+15	1.7E+15
1.87	1.7E+15	1.7E+15	1.7E+15	1.7E+15	1.7E+15	1.7E+15	1.7E+15	1.7E+15	1.7E+15
2.17	1.7E+15	1.7E+15	1.7E+15	1.7E+15	1.7E+15	1.7E+15	1.7E+15	1.7E+15	1.7E+15
2.55	1.7E+15	1.7E+15	1.7E+15	1.7E+15	1.7E+15	1.7E+15	1.7E+15	1.7E+15	1.7E+15
3.05	1.7E+15	1.7E+15	1.7E+15	1.7E+15	1.7E+15	1.7E+15	1.7E+15	1.7E+15	1.7E+15
3.80	1.7E+15	1.7E+15	1.7E+15	1.7E+15	1.7E+15	1.7E+15	1.7E+15	1.7E+15	1.7E+15
4.80	1.7E+15	1.7E+15	1.7E+15	1.7E+15	1.7E+15	1.7E+15	1.7E+15	1.7E+15	1.7E+15
6.30	1.7E+15	1.7E+15	1.7E+15	1.7E+15	1.7E+15	1.7E+15	1.7E+15	1.7E+15	1.7E+15
8.30	1.7E+15	1.7E+15	1.7E+15	1.7E+15	1.7E+15	1.7E+15	1.7E+15	1.7E+15	1.7E+15
10.80	1.7E+15	1.7E+15	1.7E+15	1.7E+15	1.7E+15	1.7E+15	1.7E+15	1.7E+15	1.7E+15
14.55	1.7E+15	1.7E+15	1.7E+15	1.7E+15	1.7E+15	1.7E+15	1.7E+15	1.7E+15	1.7E+15
19.55	1.7E+15	1.7E+15	1.7E+15	1.7E+15	1.7E+15	1.7E+15	1.7E+15	1.7E+15	1.7E+15
27.05	1.7E+15	1.7E+15	1.7E+15	1.7E+15	1.7E+15	1.7E+15	1.7E+15	1.7E+15	1.7E+15
37.05	1.7E+15	1.7E+15	1.7E+15	1.7E+15	1.7E+15	1.7E+15	1.7E+15	1.7E+15	1.7E+15
52.05	1.7E+15	1.7E+15	1.7E+15	1.7E+15	1.7E+15	1.7E+15	1.7E+15	1.7E+15	1.7E+15
72.05	1.7E+15	1.7E+15	1.7E+15	1.7E+15	1.7E+15	1.7E+15	1.7E+15	1.7E+15	1.7E+15
94.55	1.7E+15	1.7E+15	1.7E+15	1.7E+15	1.7E+15	1.7E+15	1.7E+15	1.7E+15	1.7E+15
117.05	1.7E+15	1.7E+15	1.7E+15	1.7E+15	1.7E+15	1.7E+15	1.7E+15	1.7E+15	1.7E+15
137.05	1.7E+15	1.7E+15	1.7E+15	1.7E+15	1.7E+15	1.7E+15	1.7E+15	1.7E+15	1.7E+15
154.55	1.7E+15	1.7E+15	1.7E+15	1.7E+15	1.7E+15	1.7E+15	1.7E+15	1.7E+15	1.7E+15
169.55	1.7E+15	1.7E+15	1.7E+15	1.7E+15	1.7E+15	1.7E+15	1.7E+15	1.7E+15	1.7E+15
182.05	1.7E+15	1.7E+15	1.7E+15	1.7E+15	1.7E+15	1.7E+15	1.7E+15	1.7E+15	1.7E+15
189.55	1.7E+15	1.7E+15	1.7E+15	1.7E+15	1.7E+15	1.7E+15	1.7E+15	1.7E+15	1.7E+15
194.55	1.7E+15	1.7E+15	1.7E+15	1.7E+15	1.7E+15	1.7E+15	1.7E+15	1.7E+15	1.7E+15
197.05	1.7E+15	1.7E+15	1.7E+15	1.7E+15	1.7E+15	1.7E+15	1.7E+15	1.7E+15	1.7E+15
199.30	1.7E+15	1.7E+15	1.7E+15	1.7E+15	1.7E+15	1.7E+15	1.7E+15	1.7E+15	1.7E+15
201.05	1.7E+15	1.7E+15	1.7E+15	1.7E+15	1.7E+15	1.7E+15	1.7E+15	1.7E+15	1.7E+15
202.30	1.7E+15	1.7E+15	1.7E+15	1.7E+15	1.7E+15	1.7E+15	1.7E+15	1.7E+15	1.7E+15
203.05	1.7E+15	1.7E+15	1.7E+15	1.7E+15	1.7E+15	1.7E+15	1.7E+15	1.7E+15	1.7E+15
203.55	1.7E+15	1.7E+15	1.7E+15	1.7E+15	1.7E+15	1.7E+15	1.7E+15	1.7E+15	1.7E+15

ELECTROSTATIC POTENTIAL DISTRIBUTION - IL SOLAR CELL

TERMINAL VOLTAGE = .50 V
UNIT IN VOLT

HOR-uM / VER-uM	25.00	25.02	25.27	26.02	38.52	63.52	88.52	113.52	146.02
0.00	0.50	0.56	0.57	0.54	0.45	0.44	0.44	0.44	0.44
0.05	0.43	0.46	0.48	0.45	0.37	0.35	0.35	0.34	0.34
0.10	0.37	0.38	0.41	0.38	0.31	0.29	0.29	0.28	0.28
0.15	0.31	0.32	0.34	0.32	0.25	0.24	0.23	0.23	0.23
0.20	0.26	0.26	0.29	0.27	0.21	0.19	0.19	0.19	0.19
0.25	0.21	0.22	0.23	0.22	0.16	0.15	0.15	0.15	0.15
0.30	0.16	0.16	0.17	0.16	0.12	0.11	0.10	0.10	0.10
0.37	0.11	0.11	0.11	0.10	0.07	0.07	0.07	0.06	0.06
0.47	0.07	0.07	0.07	0.06	0.05	0.04	0.04	0.04	0.04
0.60	0.05	0.05	0.05	0.04	0.03	0.03	0.03	0.04	0.04
0.75	0.03	0.03	0.03	0.03	0.03	0.03	0.03	0.03	0.03
0.92	0.02	0.02	0.02	0.01	0.01	0.01	0.02	0.02	0.02
1.12	0.01	0.01	0.01	0.01	0.01	0.01	0.01	0.01	0.01
1.35	0.00	0.00	0.00	0.00	0.00	0.00	0.00	0.00	0.00
1.60	-0.00	-0.00	-0.00	-0.00	-0.00	-0.00	-0.00	-0.00	-0.00
1.87	-0.00	-0.00	-0.00	-0.00	-0.00	-0.00	-0.00	-0.00	-0.00
2.17	-0.00	-0.00	-0.00	-0.00	-0.00	-0.00	-0.00	-0.00	-0.00
2.55	-0.00	-0.00	-0.00	-0.00	-0.00	-0.00	-0.00	-0.00	-0.00
3.05	-0.00	-0.00	-0.00	-0.00	-0.00	-0.00	-0.00	-0.00	-0.00
3.80	-0.00	-0.00	-0.00	-0.00	-0.00	-0.00	-0.00	-0.00	-0.00
4.80	-0.01	-0.01	-0.01	-0.01	-0.01	-0.01	-0.01	-0.01	-0.01
6.30	-0.01	-0.01	-0.01	-0.01	-0.01	-0.01	-0.01	-0.01	-0.01
8.30	-0.01	-0.01	-0.01	-0.01	-0.01	-0.01	-0.01	-0.01	-0.01
10.80	-0.01	-0.01	-0.01	-0.01	-0.01	-0.01	-0.01	-0.01	-0.01
14.55	-0.02	-0.02	-0.02	-0.02	-0.02	-0.02	-0.02	-0.02	-0.02
19.55	-0.03	-0.03	-0.03	-0.03	-0.03	-0.03	-0.03	-0.03	-0.03
27.05	-0.03	-0.03	-0.03	-0.03	-0.03	-0.03	-0.03	-0.03	-0.03
37.05	-0.04	-0.04	-0.04	-0.04	-0.04	-0.04	-0.04	-0.04	-0.04
52.05	-0.05	-0.05	-0.05	-0.05	-0.05	-0.05	-0.05	-0.05	-0.05
72.05	-0.05	-0.05	-0.05	-0.05	-0.05	-0.05	-0.05	-0.05	-0.05
94.55	-0.05	-0.05	-0.05	-0.05	-0.05	-0.05	-0.05	-0.05	-0.05
117.05	-0.05	-0.05	-0.05	-0.05	-0.05	-0.05	-0.05	-0.05	-0.05
137.05	-0.05	-0.05	-0.05	-0.05	-0.05	-0.05	-0.05	-0.05	-0.05
154.55	-0.04	-0.04	-0.04	-0.04	-0.04	-0.04	-0.04	-0.04	-0.04
169.55	-0.03	-0.03	-0.03	-0.03	-0.03	-0.03	-0.03	-0.03	-0.03
182.05	-0.03	-0.03	-0.03	-0.03	-0.03	-0.03	-0.03	-0.03	-0.03
189.55	-0.02	-0.02	-0.02	-0.02	-0.02	-0.02	-0.02	-0.02	-0.02
194.55	-0.02	-0.02	-0.02	-0.02	-0.02	-0.02	-0.02	-0.02	-0.02
197.05	-0.01	-0.01	-0.01	-0.01	-0.01	-0.01	-0.01	-0.01	-0.01
199.30	-0.01	-0.01	-0.01	-0.01	-0.01	-0.01	-0.01	-0.01	-0.01
201.05	-0.01	-0.01	-0.01	-0.01	-0.01	-0.01	-0.01	-0.01	-0.01
202.30	-0.00	-0.00	-0.00	-0.00	-0.00	-0.00	-0.00	-0.00	-0.00
203.05	-0.00	-0.00	-0.00	-0.00	-0.00	-0.00	-0.00	-0.00	-0.00
203.55	0.00	0.00	0.00	0.00	0.00	0.00	0.00	0.00	0.00
203.80	0.00	0.00	0.00	0.00	0.00	0.00	0.00	0.00	0.00

ELECTRON CONCENTRATION - IL SOLAR CELL

TERMINAL VOLTAGE= 0.50 V
UNIT IN ELECTRONS PER CUBIC CM

HOR-uM / VER-uM	25.00	25.02	25.27	26.02	38.52	63.52	88.52	113.52	146.02
0.00	3.1E+13	1.1E+16	3.2E+16	3.4E+16	2.0E+17	1.1E+18	1.9E+18	2.4E+18	2.6E+18
0.05	4.1E+14	3.0E+14	1.2E+15	1.4E+15	9.3E+15	3.7E+16	5.3E+16	6.1E+16	6.4E+16
0.10	3.6E+13	2.2E+13	7.0E+13	9.9E+13	8.4E+14	3.4E+15	4.8E+15	5.6E+15	5.8E+15
0.15	4.2E+12	2.8E+12	5.8E+12	9.1E+12	1.0E+14	4.4E+14	6.3E+14	7.4E+14	7.8E+14
0.20	8.9E+11	7.4E+11	9.0E+11	1.3E+12	1.6E+13	7.3E+13	1.1E+14	1.3E+14	1.4E+14
0.25	5.0E+11	4.7E+11	4.3E+11	4.9E+11	3.5E+12	1.6E+13	2.3E+13	2.8E+13	3.0E+13
0.30	4.8E+11	4.7E+11	4.2E+11	4.0E+11	7.5E+11	2.3E+12	3.3E+12	4.0E+12	4.2E+12
0.37	5.1E+11	5.0E+11	4.2E+11	3.5E+11	3.1E+11	4.7E+11	6.0E+11	6.9E+11	7.2E+11
0.47	4.8E+11	4.6E+11	3.5E+11	2.6E+11	2.7E+11	3.2E+11	3.6E+11	4.0E+11	4.1E+11
0.60	4.9E+11	4.9E+11	4.1E+11	3.3E+11	3.9E+11	4.4E+11	4.8E+11	5.1E+11	5.1E+11
0.75	3.9E+11	3.9E+11	3.9E+11	3.9E+11	4.8E+11	5.3E+11	5.6E+11	5.7E+11	5.8E+11
0.92	3.5E+11	3.5E+11	3.6E+11	3.9E+11	4.5E+11	4.8E+11	4.9E+11	5.0E+11	5.0E+11
1.12	3.9E+11	3.9E+11	4.0E+11	4.4E+11	4.7E+11	4.8E+11	4.9E+11	4.9E+11	4.9E+11
1.35	5.3E+11	5.3E+11	5.4E+11	5.7E+11	6.0E+11	6.0E+11	6.1E+11	6.1E+11	6.1E+11
1.60	7.8E+11	7.8E+11	8.0E+11	8.3E+11	8.5E+11	8.5E+11	8.5E+11	8.5E+11	8.6E+11
1.87	1.2E+12	1.2E+12	1.2E+12	1.2E+12	1.2E+12	1.2E+12	1.2E+12	1.2E+12	1.2E+12
2.17	1.8E+12	1.8E+12	1.8E+12	1.8E+12	1.8E+12	1.8E+12	1.8E+12	1.8E+12	1.8E+12
2.55	2.7E+12	2.7E+12	2.7E+12	2.7E+12	2.7E+12	2.7E+12	2.7E+12	2.7E+12	2.7E+12
3.05	4.2E+12	4.2E+12	4.2E+12	4.2E+12	4.3E+12	4.3E+12	4.3E+12	4.3E+12	4.3E+12
3.80	6.6E+12	6.6E+12	6.6E+12	6.7E+12	6.7E+12	6.7E+12	6.7E+12	6.7E+12	6.7E+12
4.80	1.1E+13	1.1E+13	1.1E+13	1.1E+13	1.1E+13	1.1E+13	1.1E+13	1.1E+13	1.1E+13
6.30	1.6E+13	1.6E+13	1.6E+13	1.6E+13	1.7E+13	1.7E+13	1.7E+13	1.7E+13	1.7E+13
8.30	2.4E+13	2.4E+13	2.4E+13	2.4E+13	2.4E+13	2.4E+13	2.4E+13	2.4E+13	2.4E+13
10.80	3.3E+13	3.3E+13	3.3E+13	3.3E+13	3.3E+13	3.3E+13	3.3E+13	3.3E+13	3.3E+13
14.55	4.3E+13	4.3E+13	4.3E+13	4.3E+13	4.3E+13	4.3E+13	4.3E+13	4.3E+13	4.3E+13
19.55	5.4E+13	5.4E+13	5.4E+13	5.4E+13	5.4E+13	5.4E+13	5.4E+13	5.4E+13	5.4E+13
27.05	6.5E+13	6.5E+13	6.5E+13	6.5E+13	6.5E+13	6.5E+13	6.5E+13	6.5E+13	6.5E+13
37.05	7.6E+13	7.6E+13	7.6E+13	7.6E+13	7.6E+13	7.6E+13	7.6E+13	7.6E+13	7.6E+13
52.05	8.7E+13	8.7E+13	8.7E+13	8.7E+13	8.7E+13	8.7E+13	8.7E+13	8.7E+13	8.7E+13
72.05	9.6E+13	9.6E+13	9.6E+13	9.6E+13	9.6E+13	9.6E+13	9.6E+13	9.6E+13	9.6E+13
94.55	1.0E+14	1.0E+14	1.0E+14	1.0E+14	1.0E+14	1.0E+14	1.0E+14	1.0E+14	1.0E+14
117.05	1.0E+14	1.0E+14	1.0E+14	1.0E+14	1.0E+14	1.0E+14	1.0E+14	1.0E+14	1.0E+14
137.05	9.7E+13	9.7E+13	9.7E+13	9.7E+13	9.7E+13	9.7E+13	9.7E+13	9.7E+13	9.7E+13
154.55	8.8E+13	8.8E+13	8.8E+13	8.8E+13	8.8E+13	8.8E+13	8.8E+13	8.8E+13	8.8E+13
169.55	7.4E+13	7.4E+13	7.4E+13	7.4E+13	7.4E+13	7.4E+13	7.4E+13	7.4E+13	7.4E+13
182.05	6.0E+13	6.0E+13	6.0E+13	6.0E+13	6.0E+13	6.0E+13	6.0E+13	6.0E+13	6.0E+13
189.55	4.6E+13	4.6E+13	4.6E+13	4.6E+13	4.6E+13	4.6E+13	4.6E+13	4.6E+13	4.6E+13
194.55	3.7E+13	3.7E+13	3.7E+13	3.7E+13	3.7E+13	3.7E+13	3.7E+13	3.7E+13	3.7E+13
197.05	2.7E+13	2.7E+13	2.7E+13	2.7E+13	2.7E+13	2.7E+13	2.7E+13	2.7E+13	2.7E+13
199.30	1.8E+13	1.8E+13	1.8E+13	1.8E+13	1.8E+13	1.8E+13	1.8E+13	1.8E+13	1.8E+13
201.05	1.1E+13	1.1E+13	1.1E+13	1.1E+13	1.1E+13	1.1E+13	1.1E+13	1.1E+13	1.1E+13
202.30	5.5E+12	5.5E+12	5.5E+12	5.5E+12	5.5E+12	5.5E+12	5.5E+12	5.5E+12	5.5E+12
203.05	1.9E+12	1.9E+12	1.9E+12	1.9E+12	1.9E+12	1.9E+12	1.9E+12	1.9E+12	1.9E+12
203.55	1.2E+05	1.2E+05	1.2E+05	1.2E+05	1.2E+05	1.2E+05	1.2E+05	1.2E+05	1.2E+05

- HOLE CONCENTRATION DISTRIBUTION - IL SOLAR CELL

TERMINAL VOLTAGE= 0.50 V

HOR-uM / VER-uM	25.00	25.02	25.27	26.02	38.52	63.52	88.52	113.52	146.02
0.00	6.8E+06	1.5E+00	1.5E+00	1.5E+00	1.2E+02	2.3E+02	2.6E+02	2.7E+02	2.7E+02
0.05	5.2E+08	4.4E+03	8.2E+01	4.3E+02	2.4E+05	9.0E+05	1.4E+06	1.7E+06	1.9E+06
0.10	8.4E+09	2.2E+06	3.0E+04	1.1E+05	3.6E+07	1.3E+08	2.1E+08	2.6E+08	2.8E+08
0.15	1.0E+11	3.3E+08	5.5E+06	1.6E+07	2.8E+09	9.1E+09	1.4E+10	1.7E+10	1.8E+10
0.20	9.4E+11	2.2E+10	5.6E+08	1.3E+09	1.2E+11	3.2E+11	4.5E+11	5.3E+11	5.6E+11
0.25	6.9E+12	7.2E+11	3.2E+10	6.3E+10	2.6E+12	5.4E+12	6.8E+12	7.7E+12	8.0E+12
0.30	7.3E+13	3.2E+13	3.8E+12	5.5E+12	5.0E+13	7.3E+13	8.3E+13	8.9E+13	9.1E+13
0.37	4.2E+14	3.5E+14	1.3E+14	1.4E+14	3.6E+14	4.2E+14	4.5E+14	4.6E+14	4.6E+14
0.47	1.1E+15	1.0E+15	7.6E+14	7.4E+14	1.0E+15	1.1E+15	1.1E+15	1.1E+15	1.1E+15
0.60	1.7E+15	1.7E+15	1.6E+15	1.5E+15	1.5E+15	1.5E+15	1.5E+15	1.5E+15	1.5E+15
0.75	1.7E+15	1.7E+15	1.7E+15	1.7E+15	1.7E+15	1.7E+15	1.7E+15	1.7E+15	1.7E+15
0.92	1.7E+15	1.7E+15	1.7E+15	1.7E+15	1.7E+15	1.7E+15	1.7E+15	1.7E+15	1.7E+15
1.12	1.7E+15	1.7E+15	1.7E+15	1.7E+15	1.7E+15	1.7E+15	1.7E+15	1.7E+15	1.7E+15
1.35	1.7E+15	1.7E+15	1.7E+15	1.7E+15	1.7E+15	1.7E+15	1.7E+15	1.7E+15	1.7E+15
1.60	1.7E+15	1.7E+15	1.7E+15	1.7E+15	1.7E+15	1.7E+15	1.7E+15	1.7E+15	1.7E+15
1.87	1.7E+15	1.7E+15	1.7E+15	1.7E+15	1.7E+15	1.7E+15	1.7E+15	1.7E+15	1.7E+15
2.17	1.7E+15	1.7E+15	1.7E+15	1.7E+15	1.7E+15	1.7E+15	1.7E+15	1.7E+15	1.7E+15
2.55	1.7E+15	1.7E+15	1.7E+15	1.7E+15	1.7E+15	1.7E+15	1.7E+15	1.7E+15	1.7E+15
3.05	1.7E+15	1.7E+15	1.7E+15	1.7E+15	1.7E+15	1.7E+15	1.7E+15	1.7E+15	1.7E+15
3.80	1.7E+15	1.7E+15	1.7E+15	1.7E+15	1.7E+15	1.7E+15	1.7E+15	1.7E+15	1.7E+15
4.80	1.7E+15	1.7E+15	1.7E+15	1.7E+15	1.7E+15	1.7E+15	1.7E+15	1.7E+15	1.7E+15
6.30	1.7E+15	1.7E+15	1.7E+15	1.7E+15	1.7E+15	1.7E+15	1.7E+15	1.7E+15	1.7E+15
8.30	1.7E+15	1.7E+15	1.7E+15	1.7E+15	1.7E+15	1.7E+15	1.7E+15	1.7E+15	1.7E+15
10.80	1.7E+15	1.7E+15	1.7E+15	1.7E+15	1.7E+15	1.7E+15	1.7E+15	1.7E+15	1.7E+15
14.55	1.7E+15	1.7E+15	1.7E+15	1.7E+15	1.7E+15	1.7E+15	1.7E+15	1.7E+15	1.7E+15
19.55	1.7E+15	1.7E+15	1.7E+15	1.7E+15	1.7E+15	1.7E+15	1.7E+15	1.7E+15	1.7E+15
27.05	1.7E+15	1.7E+15	1.7E+15	1.7E+15	1.7E+15	1.7E+15	1.7E+15	1.7E+15	1.7E+15
37.05	1.7E+15	1.7E+15	1.7E+15	1.7E+15	1.7E+15	1.7E+15	1.7E+15	1.7E+15	1.7E+15
52.05	1.7E+15	1.7E+15	1.7E+15	1.7E+15	1.7E+15	1.7E+15	1.7E+15	1.7E+15	1.7E+15
72.05	1.7E+15	1.7E+15	1.7E+15	1.7E+15	1.7E+15	1.7E+15	1.7E+15	1.7E+15	1.7E+15
94.55	1.7E+15	1.7E+15	1.7E+15	1.7E+15	1.7E+15	1.7E+15	1.7E+15	1.7E+15	1.7E+15
117.05	1.7E+15	1.7E+15	1.7E+15	1.7E+15	1.7E+15	1.7E+15	1.7E+15	1.7E+15	1.7E+15
137.05	1.7E+15	1.7E+15	1.7E+15	1.7E+15	1.7E+15	1.7E+15	1.7E+15	1.7E+15	1.7E+15
154.55	1.7E+15	1.7E+15	1.7E+15	1.7E+15	1.7E+15	1.7E+15	1.7E+15	1.7E+15	1.7E+15
169.55	1.7E+15	1.7E+15	1.7E+15	1.7E+15	1.7E+15	1.7E+15	1.7E+15	1.7E+15	1.7E+15
182.05	1.7E+15	1.7E+15	1.7E+15	1.7E+15	1.7E+15	1.7E+15	1.7E+15	1.7E+15	1.7E+15
189.55	1.7E+15	1.7E+15	1.7E+15	1.7E+15	1.7E+15	1.7E+15	1.7E+15	1.7E+15	1.7E+15
194.55	1.7E+15	1.7E+15	1.7E+15	1.7E+15	1.7E+15	1.7E+15	1.7E+15	1.7E+15	1.7E+15
197.05	1.7E+15	1.7E+15	1.7E+15	1.7E+15	1.7E+15	1.7E+15	1.7E+15	1.7E+15	1.7E+15
199.30	1.7E+15	1.7E+15	1.7E+15	1.7E+15	1.7E+15	1.7E+15	1.7E+15	1.7E+15	1.7E+15
201.05	1.7E+15	1.7E+15	1.7E+15	1.7E+15	1.7E+15	1.7E+15	1.7E+15	1.7E+15	1.7E+15
202.30	1.7E+15	1.7E+15	1.7E+15	1.7E+15	1.7E+15	1.7E+15	1.7E+15	1.7E+15	1.7E+15
203.05	1.7E+15	1.7E+15	1.7E+15	1.7E+15	1.7E+15	1.7E+15	1.7E+15	1.7E+15	1.7E+15
203.55	1.7E+15	1.7E+15	1.7E+15	1.7E+15	1.7E+15	1.7E+15	1.7E+15	1.7E+15	1.7E+15

REFERENCES

1. G. C. Salter and R. E. Thomas, "Silicon Solar Cells Using Natural Inversion Layer Found in Thermally–Oxidized p–Silicon," Solid State Electronics, Vol. 20, pp. 95–104, 1977.

2. C. E. Norman and R. E. Thomas, "Detailed Modeling of Inversion Layer Solar Cells," IEEE Trans. Electron Devices, Vol. ED–27, pp. 731–737, 1980.

3. R. B. Godfrey and M. A. Green, "High–Efficiency Silicon MinMIS Solar Cells – Design and Experimental Results," IEEE Trans. Electron Devices, Vol. ED–27, pp. 737–745, 1980.

4. W. A. Miller and L. C. Olson, "Model Calculations for Silicon Inversion Layer Solar Cells," pp. 371–395, 1983.

5. J. D. Plummer and B. E. Deal, "Thermal Oxidation: Kinetics, Charges, Physical Models, and Interaction with Other Process in VLSI Devices," Process and Device Simulation for MOS–VLSI Circuits, P. Antognetti, D. A. Antoniadis, R. W. Dutton and W. G. Oldham, Eds., (Martinus Nijhoff Publishers, Boston, 1983), pp. 44–87.

6. A. DeMari, "An Accurate Numerical Steady–State One–Dimensional Solution of the p–n junction," Solid State Electronics, 11, pp. 33–58, 1968.

7. A DeMari, "An Accurate Numerical One–Dimensional Solution of the p–n Junction Under Arbitrary Transient Conditions," Solid State Electronics, 11, pp. 2021–2053, 1968.

8. H. K. Gummel, "A Self–Consistent Iterative Scheme for One–Dimensional Steady State Transistor Calculations," IEEE Trans. Electron Devices, Vol. ED–11, pp. 455–465, 1964.

9. H. L. Stone, "Iterative Solution of Implicit Approximations of Multidimensional Partial Differential Equations," SIAM J. Numer. Anal., Vol. 5, pp. 530–558, 1968.